Advances in Colloid and Interface Science 226 (2015) 123–137

Contents lists available at ScienceDirect

Advances in Colloid and Interface Science

journal homepage: www.elsevier.com/locate/cis

Historical perspective

Near-infrared light activated delivery platform for cancer therapy

Min Lin [a,b,c,*], Yan Gao [a], Francis Hornicek [a], Feng Xu [b,c], Tian Jian Lu [b,c], Mansoor Amiji [d], Zhenfeng Duan [a,*]

[a] Center for Sarcoma and Connective Tissue Oncology, Massachusetts General Hospital, Harvard Medical School, MA 02114, USA
[b] The Key Laboratory of Biomedical Information Engineering, Ministry of Education, School of Life Science and Technology, Xi'an Jiaotong University, Xi'an 710049, PR China
[c] Bioinspired Engineering and Biomechanics Center (BEBC), Xi'an Jiaotong University, Xi'an 710049, PR China
[d] Department of Pharmaceutical Sciences, School of Pharmacy, Northeastern University, Boston, MA 02115, USA

ARTICLE INFO

Available online 14 October 2015

Editor: A. Amirfazli

Keywords:
Upconversion nanoparticle
Payload encapsulation strategies
Photoactivation
Controlled delivery
Cancer therapy

ABSTRACT

Cancer treatment using conventional drug delivery platforms may lead to fatal damage to normal cells. Among various intelligent delivery platforms, photoresponsive delivery platforms are becoming popular, as light can be easily focused and tuned in terms of power intensity, wavelength, and irradiation time, allowing remote and precise control over therapeutic payload release both spatially and temporally. This unprecedented controlled delivery manner is important to improve therapeutic efficacy while minimizing side effects. However, most of the existing photoactive delivery platforms require UV/visible excitation to initiate their function, which suffers from phototoxicity and low level of tissue penetration limiting their practical applications in biomedicine. With the advanced optical property of converting near infrared (NIR) excitation to localized UV/visible emission, upconversion nanoparticles (UCNPs) have emerged as a promising photoactive delivery platform that provides practical applications for remote spatially and temporally controlled release of therapeutic payload molecules using low phototoxic and high tissue penetration NIR light as the excitation source. This article reviews the state-of-the-art design, synthesis and therapeutic molecular payload encapsulation strategies of UCNP-based photoactive delivery platforms for cancer therapy. Challenges and promises for engineering of advanced delivery platforms are also highlighted.

Contents

* Co-corresponding authors.
E-mail addresses: minlin@mail.xjtu.edu.cn (M. Lin), ZDUAN@mgh.harvard.edu (Z. Duan).

http://dx.doi.org/10.1016/j.cis.2015.10.003
0001-8686/

1. Introduction

Cancer is a major public health issue with over 1.6 million new cases and almost 600,000 deaths occurring in the United States in 2014 [1]. Significant toxicity to normal tissues and development of drug resistance in tumor cells are two major obstacles for current cancer chemotherapy. Short circulation times of most chemotherapy drugs and difficulty of localization to tumor sites further challenge current cancer therapies. Normal cell damage induced by chemotherapy can, in some cases, even be fatal. The almost universal development of multidrug resistance (MDR) by tumor cells is responsible for the majority of treatment failures in clinic. Overcoming these challenges associated with current cancer treatments has been a high priority goal of clinical and basic scientists, but remains an elusive outcome.

In recent years, nanotechnology has been successfully applied in vitro and in animal models in vivo to overcome these hurdles in cancer therapy. Nanotechnology is quickly becoming a promising innovation in cancer treatment for the future. With new advances in nanotechnology, nanoparticle based controlled drug delivery systems may find wide applications in various cancer therapies. The delivery of therapeutic payload using engineered micro/nanomaterial-based delivery systems, such as polymeric micelles [2,3], dendrimers [4,5], meso-porous silica [6,7], gold nanoparticles [8], and ion oxide nanoparticles [9,10], has attracted increasing attention. While these delivery systems are extremely valuable, they suffer from irregular release and notched distribution of payloads in physiological conditions leading to adverse reactions. Ideal delivery systems entail "zero-release" before reaching the targeted biosites and controlled release of the therapeutic payloads. With the development of various stimuli-responsive delivery platforms, greater control over the delivery and release processes in either temporal or spatial manners have been made possible. Several release strategies have been developed, including low pH [11,12], high enzyme concentration [13], redox materials within the cells [14], and the use of light as external stimulus [15]. Among these strategies, light activation offers unprecedented control over others. Light of specific wavelength allows remote, noninvasive, spatial, and temporal control over photoactive delivery platforms, enabling greater safety, specificity, and therapeutic efficacy. Despite numerous benefits, the majority of the existing photoactive delivery platforms require ultraviolet (UV) or short visible light as external excitation sources, which inevitably involve cellular phototoxicity and poor tissue penetration depth resulting in limited clinical potential.

Alternatively, upconversion nanoparticles (UCNPs) feature advanced optical properties enabling conversion of near infrared (NIR) excitation to localized UV/visible emission. High tissue penetration and low photo energy of NIR endow UCNPs with many advantages over quantum dots and organic fluorescent materials in biological applications, such as low photodamage and enhanced tissue penetration [16,17], minimal autofluorescence background [18], and improved resistance to photobleaching and blinking [19]. These intrinsic upconversion luminescence properties provide many unprecedented opportunities for UCNPs to serve as nanotransducers to substitute the undesired direct UV/visible excitation with NIR excitation. This potentiates remote, "on demand" NIR photoactivated therapeutic payload release with high spatial and temporal resolution, allowing for the design and optimization of photoactivated delivery at a desired location and specific time. Accumulating evidences show that UCNP-based photoactive delivery platforms have been engineered for NIR activated therapeutic applications, including chemotherapeutic drugs [20–22], gene therapy [23–25], photodynamic therapy [20,26,27], and photothermal therapy [20,28,29].

In the past few years, investigations on design and synthesis of UCNPs and their bioapplications, including drug delivery, theranostics, biodetection, and bioimaging, have been of increasing interest [30–43]. This rapid development of UCNPs in biological applications necessitates a thorough state-of-the-art review focusing on the most recent advances in UCNP-based NIR activated delivery platform for cancer therapy. Our review article elaborates on the following topics: In Section 2, engineering of upconversion based photoactivative delivery system is presented, with emphasis on recent advances in therapeutic molecules encapsulation strategies. For this, we first illustrate the mechanism of upconversion luminescence and the principle of dopant/host selection criteria for design of UCNPs. Two representative synthesis routes are discussed with advantages and disadvantages. Surface chemistry for aqueous solubility, bioconjugation, and targeting capabilities are then summarized. Various strategies for therapeutic molecule encapsulation are highlighted. Section 3 focuses on the application of UCNP-based NIR activated delivery platforms for cancer therapies, including chemotherapy, gene therapy, photodynamic therapy, and photothermal therapy. Section 4 summarizes limitations associated with current progress and envisions the prospective bioapplications of UCNPs by highlighting areas with exceptional promise and challenges.

2. Engineering of upconversion nanoparticle based photoactive delivery system

Applications of UCNPs as a photoactive delivery system demand precise control over synthetic strategies, including high crystallinity, monodispersed size and morphology, good solubility in aqueous solution, and suitable functional groups on the surface that allow further conjugation or targeting capabilities. The following sections will review the design principles of UCNPs, surface chemistry for aqueous solubility, and bioconjugation. Emphasis will be placed on payload encapsulation strategies.

2.1. Design of UCNPs with superior optical properties

Upconversion luminescence refers to a unique process defined by sequential absorption of two or more photons with low-energy at a long wavelength, followed by the emission of photons with higher energy at a shorter wavelength [44]. The mechanism of upconversion luminescence can be classified into three groups: excited state absorption (ESA), energy transfer upconversion (ETU), and photon avalanche (PA) [45]. Among these three processes, ETU is instantaneous and pump power independent (Fig. 1 A), and is widely used to offer efficient upconversion luminescence (~ two orders of magnitude higher than ESA) [45].

To achieve upconversion luminescence, lanthanide-doped UCNPs are mainly composed of crystalline hosts and lanthanide dopants, which incorporate into to the host lattice at low concentrations [45]. The ion that emits fluorescence is the activator, while the donator of the energy is the sensitizer. In the case of sensitized luminescence, the activator radiates upon its excitation to a higher energetic state obtained from the non-radiative transfer of the energy from sensitizer. In principle, efficient upconversion luminescence only occurs by well selected dopant-host combinations. The dopant selection criteria is based on the characteristic spaced energy levels that render photon absorption by sensitizer and subsequent energy transfer between the sensitizer and activator in the upconversion process [46]. Due to its high absorption coefficient and upconversion efficiency, Yb^{3+} is usually selected as the sensitizer [47]. Er^{3+} and Tm^{3+} are most frequently used as activators, which possess ladder-like energy levels and are well resonant with non-radiative multiphonon relaxation from Yb^{3+}, enabling efficient energy transfer from Yb^{3+} to these ions (Fig. 1 B) [45]. Fluorides usually exhibit low phonon energies (~350 cm^{-1}) and high chemical stability, and thus are widely used as host materials [48–50].

2.2. Synthesis strategies

A variety of methods, including thermal decomposition [49,51–57], hydro(solvo)thermal synthesis [58–65], co-precipitation [50,62,66–68], sol–gel process [69–73], and combustion synthesis [74–76],

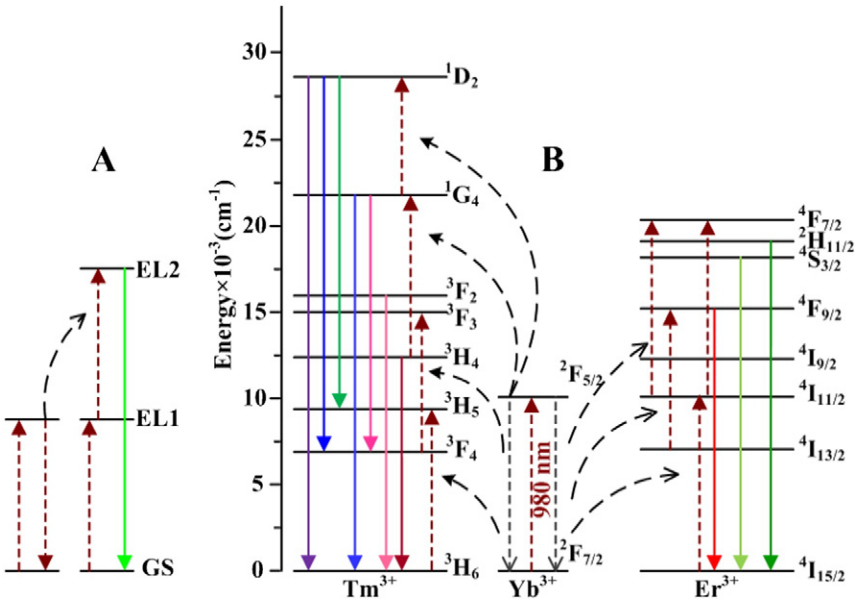

Fig. 1. Illustration of upconversion emission. Schematic of energy transfer upconversion (ETU) (A). Upconversion emission scheme of the Yb^{3+} sensitized Er^{3+} and Tm^{3+} co-doped system (B). GS: ground state; EL: energy level.

have been developed to synthesize lanthanide-doped UCNPs with controlled crystalline phases and sizes. Previous reviews have reported on various innovative synthesis routes [31–33,39,45,77]. Among these methods, thermal decomposition and hydro(solvo)thermal synthesis routes are the two most popular methods for preparing UCNPs, which are commonly used for biomedical applications.

Hydro(solvo)thermal synthesis is a typical solution-based approach, which exploits water or a solvent under elevated temperatures and pressures above its critical point to facilitate reaction of the dissolved material/precursor ions and subsequent crystallization [61,62,78,79]. Hydrothermal methods have been shown to be effective in synthesizing β-$NaYF_4$ based UCNPs with controlled morphologies, including nanosphere [64], nanowires [80], microrod [65], microprim [81], pindle-like microcrystal [82], and octadecahedron [83]. The morphologies of particles have significant effects on their fluorescence properties [65,84,85]. Compared with the toxicity of using organic solvents for particle synthesis, a water-based system provides a relatively green chemical alternative for the preparation of UCNPs [86]. The advantages associated with the hydro(solvo)thermal method include easily controllable reaction conditions, a relatively low cost and high yield, a relatively low reaction temperature (in general < 250 °C), and easily controlled size, structure, and shapes of the products [28]. The reaction conditions, such as reactant concentration, type and concentration of doped ions, hydrothermal temperature and time, and pH, can influence the growth of the nanocrystals [87,88]. Particularly, control of the doping ion (e.g., Gd^{3+}) has also been demonstrated to affect crystallographic phase, size, and upconversion emission of UCNPs [89].

Highly monodispersed UCNPs with smaller sizes can be synthesized by a thermal decomposition process, which involves thermolysis of rare earth precursors in high-boiling organic solvents (e.g., oleic acid (OA), oleylamine (OM), octadecene (ODE)) at high temperature (usually exceeding 300 °C) [49,55,57,90–92]. Pioneer work on the synthesis of highly monodispersed UCNPs was done by Yan's group who prepared $NaYF_4$:Yb,Er, $NaYF_4$:Yb,Tm, $LiYF_4$:Yb,Er, and $KGdF_4$:Yb,Er by decomposition of multiprecursors of Na(CF3COO), $Y(CF3COO)_3$, $Yb(CF3COO)_3$, $Er(CF3COO)_3$, $Tm(CF3COO)_3$, $Li(CF_3COO)$, and $K(CF_3COO)$ in OA/OM/ODE solvents (representative TEM images, Fig. 2 A, B) [53,54,56,87,93]. Around the same time, Capobianco's group and Chow's group also reported the synthesis of UCNPs via the thermal decomposition method. For example, Capobianco and co-workers reported the synthesis of $NaYF_4$ nanoparticles co-doped with Yb/Er or Yb/Tm via thermal decomposition of metal trifluoroacetate precursors in the presence of OA and ODE [57]. They refined this technique to synthesize UCNPs with a remarkably narrow size distribution [49]. Hexagonal-phase $NaYF_4$:Yb,Er and $NaYF_4$:Yb,Tm nanoparticles with an average particle size of 10.5 nm and core/shell structure with much higher upconversion fluorescence were obtained by Chow's group [48,55].

More recently, considerable efforts have been devoted to the synthesis of UCNPs with specific emission and excitation wavelengths via thermal decomposition route [43]. For photoactivated therapeutic applications of UV emission [23,25,94], the goal is to maintain deep tissue penetration while keeping the excitation wavelength where the water absorption induced heat effect is negligible (e.g., 800 nm) [95–97]. For NIR-to-UV emission, Yb/Tm doped $NaYF_4$ and YF_3 nanoparticles with uniform size distributions have been developed [53,94]. To achieve higher UV emission, a two-step thermal decomposition method has also been applied to the synthesis of advanced core–shell UCNPs as $NaGdF_4$:Yb/Tm@$NaGdF_4$ [98,99] and NaYF4:Yb/Tm@CaF_2 (Fig. 2C, D) [100]. Despite synthesis of UCNPs with tuned emission, the excitation wavelength also needs to be fine-tuned to ~800 nm to avoid heat effect. For instance, tri-doped $NaYF_4$:Nd,Yb,Er(Tm)@$NaYF_4$ core/shell UCNPs with a biocompatible excitation wavelength of 800 nm were successfully developed [101]. These UCNPs show lower heating effect, given the same upconversion emission intensity [101]. Similarly, $NaGdF_4$:Nd/Yb/Er and $NaGdF_4/Nd_3$@$NaGdF_4$/Tm/Yb core–shell UCNPs with a sharp absorption peak centered around 800 nm have also been synthesized [102,103]. The limitation for this method is that the doping concentration of Nd^{3+} is typically below 3%. The low doping concentration leads to weak absorption capacity at 800 nm resulting in weak upconversion emission intensity [101–103]. An improved structure based on an energy migration mechanism has been proposed by Liu's group through coating of core NaYF4:Yb/Tm/Nd with high-concentration doping of Nd^{3+} (~20 mol%) in the shell layer (Fig. 2 E, F) [95]. The prepared $NaYF_4$:Yb/Tm/Nd@$NaYF_4$:Nd core–shell UCNPs produced enhanced emission intensity by ~405 times higher than that without the shell coating [95].

2.3. Surface chemistry and bioconjugation

Though UCNPs with controlled and uniform size, morphology has been successfully synthesized through different methods as introduced in the previous section, these UCNPs are usually hydrophobic due to the

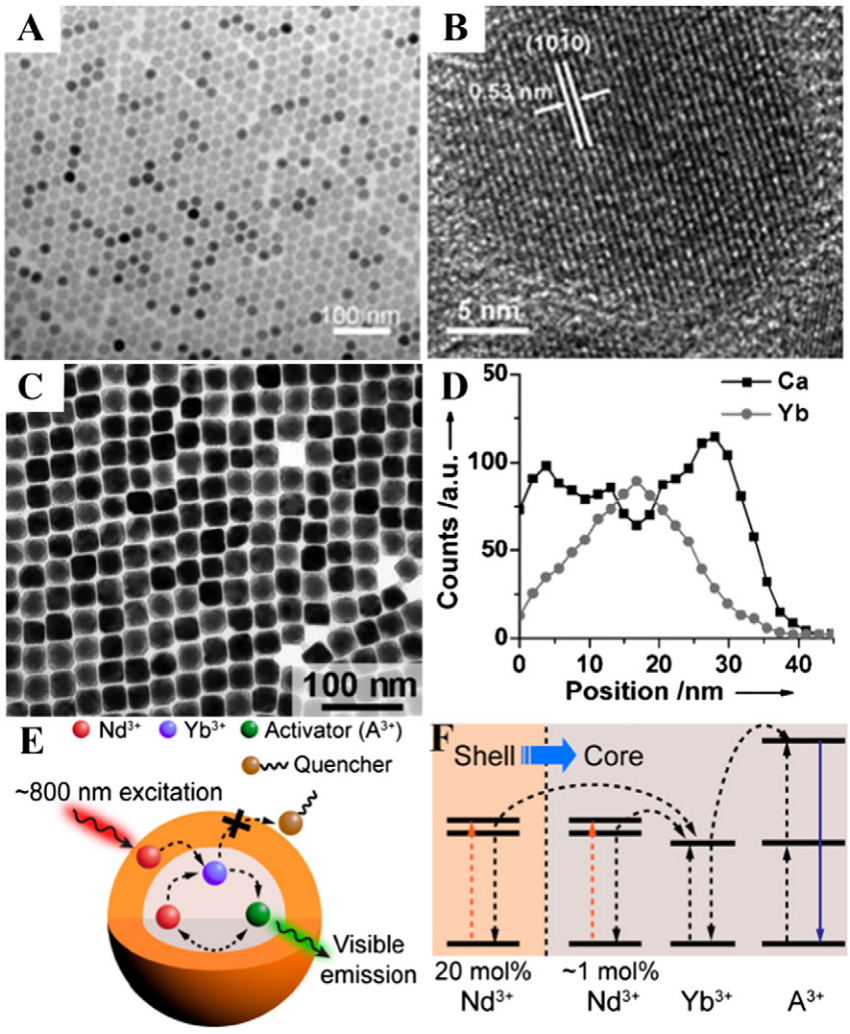

Fig. 2. TEM images of UCNPs and energy migration in core–shell UCNPs for enhanced emission. TEM image of β-$NaYF_4$:Yb,Tm nanoparticles (A). Higher magnification (B) [53]. Reprinted with permission from Anxiang Yin, Yawen Zhang, Lingdong Sun, Chunhua Yan, Nanoscale, 2010, 2(6), 953–959. Copyright 2010 Royal Society of Chemistry. TEM image (C) and elemental ratio analysis by linear EDX scanning of a single α-$NaYbF_4Tm$@CaF_2 demonstrating CaF_2 coating (D) [100]. Reprinted with permission from Jie Shen, Guanying Chen, Tymish Y. Ohulchanskyy, Samuel J. Kesseli, Steven Buchholz, Zhipeng Li, Paras N. Prasad, Gang Han, Small, 2013, 9(19), 3213–3217. Copyright 2013 John Wiley and Sons. Illustration of a core–shell nanoparticle (E) and corresponding mechanism of energy migration for enhanced photon upconversion emission (F) [95]. Reprinted with permission from Xie, Xiaoji Gao, Nengyue, Deng, Renren, Sun, Qiang, Xu, Qing-Hua, Liu, Xiaogang, Journal of the American Chemical Society, 2013, 135(34), 12,608–12,611. Copyright 2013 American Chemical Society.

OA-coating (resulting from the organic solvent) on the surface. Surface modification of UCNPs plays a crucial role to improve their aqueous solubility for subsequent bioapplications. To obtain hydrophilic UCNPs, numerous efforts have therefore been devoted to the development of different surface chemistry strategies, including polymer capping, surface silanization, surface ligand oxidation, ligand exchange, and amphiphilic polymer coating. One-step synthesis of polymer capping hydrophilic UCNPs have been achieved by introducing 6-aminohexanoic acid (AA) and oleic acid (OA) as binary cooperative ligands in hydrothermal reactions [104]. The carboxylic acid group from AA bonds to the lanthanide ions and its amino group stretch out facilitating water solubility. Increasing the molar ratio of AA contributes to improved water-solubility of the UCNPs-OA/AA. Similarly, poly(ethylene glycol) (PEG) and OA have also been employed as binary cooperative ligands to improve the water-solubility of UCNPs in a one-step hydrothermal reaction process [105], controlling the amount of poly(ethyleneglycol) bis(carboxymethyl)ether and producing hydrophilic small sized (~8 nm) UCNPs.

Silica coating via surface silanization of UCNPs is a well-established strategy for obtaining aqueous soluble UCNPs [106–109]. Silica coating is of great importance for improved aqueous solubility and biocompatibility. Besides, the existence of $-NH_2$ (could be easily introduced in the coating procedure) facilitates further conjugation with biological moieties. Furthermore, a mesoporous silica coating with tunable pore size not only improves its solubility in aqueous solutions, but also it is capable of loading biomoleculars or therapeutic payload drugs due to its large surface area [110,111]. Alternatively, other methods employing ligand oxidation reaction [112–115], ligand exchange [116,117], and amphiphilic polymer coating [118,119] are also attractive for improving aqueous solubility of UCNPs.

Beside aqueous solubility, surface functionalization of UCNPs by bioconjugation chemistry is of particular importance for target specificity (e.g., imaging, delivery) by adding targeting agents, including folic acid, antibodies, peptides, and other targeting ligands. Among these targeting agents, folic acid (FA) has been most commonly exploited as targeting agent due to the overexpression of folic acid receptor in many human cancer cells. Folate receptor mediated binding of FA conjugated UCNPs has been demonstrated in various cancer cells, including murine sarcoma tumor S180 cells [120], murine melanoma B16F0 cells [121], human hepatocellular carcinoma Bel-7402 cells, human breast cancer MCF-7 cells [112], human cervical cancer HeLa cells [122], human nasopharyngeal epidermal carcinoma KB cells, human colon cancer HT29 cells [123], and human choriocarcinoma JAR cells [124]. High specificity and affinity of FA to folate receptors enhance targeted cell uptake in a non-destructive, endocytotic manner. Targeting cancer cells or tumor

vasculature with peptides and antibodies is another promising strategy for targeted delivery of UCNPs based therapeutic nanoplatforms. Other targeting ligands, for example, 3-aminophenylboronic acid (APBA) and hyaluronic acid (HA), have also been reported to respectively target polysialic acid and cluster determinant 44 (CD44) receptors for dual targeting applications [125]. Single-stranded oligonucleotides called aptamers have also emerged as a novel targeting moiety for functionalization of UCNPs [126].

2.4. Therapeutic payload molecule encapsulation strategies

For successful encapsulation of payload molecules into photoactive delivery systems, several design criteria need to be met, including: (i) avoiding premature loss of payload molecules before the delivery system can reach its target site; (ii) loading of necessary amount of photosensitizer to avoid self-quenching of the generated reactive oxygen species in photodynamic treatments; and (iii) light activated controlled release kinetics of payload molecules from the delivery system. Accordingly, several encapsulation strategies have been applied for NIR induced remote controlled release/monitoring of payload molecules. These strategies can be classified into the following categories: (1) physical encapsulation/absorption; (2) encapsulation by photolabile groups; and (3) encapsulation by photochromic compounds. Recent reports on upconversion-based photoactive delivery platform using those different strategies are summarized in Table 1.

1) Physical encapsulation/absorption
UCNPs with a porous silica coating are an attractive drug delivery platform due to their highly specific surface area in the silica layer that facilitates physical encapsulation of payload molecules. The first attempt to physically encapsulate a photosensitizer molecule using dense silica coated UCNPs for photodynamic therapy application was demonstrated by Zhang et al. [127] and Shi et al. [28]. However, the negatively charged and hydrophilic properties of the silica layer have unfavorable effects in encapsulation of an anionic, hydrophobic photosensitizer resulting in low loading capacity of only 0.46 wt.% [127]. On the contrary, methylene blue (MB)/UCN exhibited a greater loading capacity of 0.05 mmol due to the strong absorption of water-soluble, cationic MB into the silica matrix [28]. Besides dense silica coating, mesoporous silica coating with even larger pore size (2–50 nm) and higher surface area enables greater loading capacities [128,129]. The high loading level of nucleic acids into mesoporous silica was observed to range between ~75.4 to ~111.5 mg/g as compared with that of dense silica which ranged between ~40 to ~50 mg/g [130]. Similar to dense silica, the high encapsulation capacity of mesoporous silica is also restricted to cationic, hydrophilic payload molecules. Loading of hydrophobic payload molecules (e.g., ZnPc, MC540) into mesoporous silica is typically lower (<0.5 wt.%) [128,121,131].
As an alternative of absorption by silica coating, physical adsorption via electrostatic attraction as another loading strategy has also been developed for UCNP-based delivery systems [26,132,133,134]. Most recently, Liu et al. adopted this method for loading of UCNPs using the layer-by-layer assembly process (Fig. 3A, B) [26]. Ce6 was conjugated by poly (allylamine hydrochloride) (PAH) to form a negatively charged Ce6-conjugated polymer. Loading of Ce6 was realized by the electrostatic attraction between negatively charged Ce6-conjugated polymer and positively charged UCNP/PAA/PAH. The adhesion between Ce6 and UCNPs is strong enough that there was minimal leakage of Ce6 within 48 h under physiological conditions. This encapsulation strategy provides a high Ce6 loading capacity of 3.4 wt.%, 7.7 wt.%, and 11.0 wt.% for different layers of the negatively charged Ce6-conjugated polymer.

2) Encapsulation by photolabile groups
Though loading capacity has been greatly improved, the major disadvantage associated with payload molecules encapsulated by physical absorption is the irregular payload release or burst release in the initial stage. Payload release in a light-controllable manner has been developed through caging of therapeutic compounds with photolabile groups, and then subsequently uncaging under photoactivated degradation of the groups [22,135,136]. A number of photolabile groups have been employed, including NB [136], NE [137], NBA [21], di(carboxymethoxy)benzoin [138], OBN [139,140], DMNPE [25], and ONA [141] for caging of different payloads. For instance, Liu and colleagues designed crosslinked mesoporous silicacoated UCNPs as nanovehicles for photoactive gene delivery [23]. In their work, $NaYF_4$:Yb/Tm UCNPs were coated with a silica layer and were then functionalized with a cationic photolabile group through covalent bonding. Negatively charged siRNA was conjugated onto the nanovehicle through electrostatic interactions. Since the spectra overlap between the absorption band of photolabile group and the localized UV emission band of the UCNPs, irradiation with NIR light triggered the cleavage of the photolabile group resulting in the release of siRNA from the nanovehicle. However, a very low loading capacity of 0.7 wt.% was achieved by this strategy. To overcome this problem, Li's group developed a novel $NaYF_4$:Yb/Tm@$NaLuF_4$ based yolk–shell structure as a photoactive delivery system (Fig. 3C, D) [142]. The hollow cavities in the nanostructure provide a large loading capacity (49 wt.%, 5.3×10^6 molecules per particle) for payload molecules enabling a sustainable release characteristic. Prior to loading into the yolk–shell nanostructure, the chlorambucil was caged by the photolabile group of an aminocoumarin derivative (ACCh). Upon NIR excitation, UV emission from the UCNPs cleaves the aminocoumarin derivative, resulting in the uncaging and releasing of the chlorambucil from the nanostructure.

3) Encapsulation by photochromic compounds
Another effective light-responsive encapsulation method is by use of photochromic compounds, which are able to switch between two structurally and electronically different isomers under UV–Vis light activation. As a representative photochromic compound, the azobenzene group (and its derivatives) has been demonstrated to be capable of photoactive control of drug release [143]. By similar concept, different photochromic compounds, such as Azobenzenes [22], Spiropyrans [144], Diarylethenes [145], Diarylethenes [146], Diarylethenes [147], Bis-spiropyrans [148], and Azobenzene derivatives [149], have been applied for upconversion based photoactive delivery systems. Representative example of NIR light activated DOX release based on photoswitching of the azobenzene modified mesoporous silica coated UCNPs has been reported by Shi et al. [22]. In their study, photoactive azobenzene molecules were incorporated into the mesopores of silica layer (Fig. 3E, F). Under NIR excitation, UV and visible emissions from UCNPs overlap with the absorption of azobenzene molecules causing reversible trans-cis photoisomerization of the azobenzene molecules within the mesopores in silica layer. This reversible photoisomerization provides rotation–inversion movement resembling "wagging motion" that renders the release of DOX molecules. Their further in vitro experiments demonstrated that DOX release can be well regulated by NIR irradiation with various intensities and time durations.

3. Applications of upconversion-based photoactivated cancer therapeutics

A UCNP-based delivery system is capable of converting NIR light to UV light, subsequently activating the photoactive compounds to release the payload upon NIR excitation. This unique characteristic has been adopted for design of various delivery systems for controlled payload release upon NIR irradiation, including generated heat in photothermal therapy. The following sections will review a set of NIR activated UCNP-based smart delivery systems for advanced therapeutic applications,

Table 1
Upconversion-based photoactive delivery platform.

Payload encapsulation strategies	UCNP core (size)	Surface coating	Photoactivatable group type	Delivery nanostructure	Payload (drug/gene)	Cancer cell/animal model type	Targeting agent	Activation wavelength (Emission from UCNPs, nm)	In vitro/vivo	Ref.
Physical encapsulation/absorption	$NaYF_4$:Yb/Er (60 nm–120 nm)	SiO_2	None	$NaYF_4$:Yb/Er@SiO_2	M-540	MCF-7/AZ cells	MUC1/episialin antibody	537	In vitro	[127]
	$NaYF_4$:Er/Yb/Gd (50 nm)	SiO_2	None	$NaYF_4$:Er/Yb/Gd@SiO_2	MB	None	None	651	None	[28]
	$NaYF_4$:Yb/Er (width: 35 nm; length: 60 nm)	$mSiO_2$	None	$NaYF_4$:Yb/Er@ $mSiO_2$	ZnPc	MB49 cells	None	645–670	In vitro	[172]
	$NaYF_4$:Yb/Er (~100 nm)	$mSiO_2$, PEG	None	$NaYF_4$:Yb/Er@ $mSiO_2$@PEG	M-540, ZnPc	B16-F0 cells, B16-F0 melanoma cell mouse model	FA	540, 660	In vitro, In vivo	[121]
	$NaYF_4$:Yb/Er (50 nm)	$mSiO_2$	None	$NaYF_4$:Yb/Er@ $mSiO_2$	ZnPc	MB49 cells	None	645–670	In vitro	[173]
	$NaYF_4$:Yb/Tm (30–60 nm)	$NaYF_4$:Yb/Er, SiO_2, $mSiO_2$	TPPSa	$NaYF_4$:Yb/Tm@ $NaYF_4$:Yb/Er@ SiO_2 @$mSiO_2$	anti-STAT3	B16-F0 cells, B16-F0 melanoma cell mouse model	None	330–370, 413	In vitro, In vivo	[24]
	$NaY(Mn)F_4$:Yb/Er (20 nm)	PAA, PAH, DMMA, PEG	None	$NaY(Mn)F_4$:Yb/Er@PAA@PAH@DMMA@PEG	Ce6	HeLa cells, 4 T1 murine breast tumor model	None	660	In vitro, In vivo	[26]
Encapsulated by photolabile groups	$NaYF_4$:Yb/Tm (55 nm)	$NaYF_4$, $mSiO_2$	NB	$NaYF_4$:Yb/Tm@$NaYF_4$@$mSiO_2$	DOX	A-498 cells, HeLa cells, NIH/3 T3 cells	FA	350	In vitro	[136]
	$NaYF_4$:Yb/Tm(~35 nm)	SiO_2	NBA	$NaYF_4$:Yb/Tm@SiO_2	DOX	HeLa cells, A549 cells, MRC-5 cells, HeLa cancer cell mouse tumor model	FA	360	In vitro, In vivo	[21]
	$NaYF_4$:Yb/Tm (25 nm)	SiO_2, $mSiO_2$	DMNPE	$NaYF_4$:Yb/Tm@SiO_2/$mSiO_2$	siRNA, Plasmid DNA	B16-F0 cells	None	350	In vitro	[25]
	$NaYF_4$:Yb/Tm (~30 nm)	$NaLuF_4$, YS	Amino-coumarin	$NaYF_4$:Yb/Tm@$NaLuF_4$	Chlorambucil	KB cells, murine sarcoma 180 model	None	345, 362	In vitro, In vivo	[142]
	$NaYF_4$:Yb/Tm (65 nm)	SiO_2	*o*-nitrobenzyl groups	$NaYF_4$:Yb/Tm@SiO_2	Alexa-siRNA	HeLa cells	None	350–360	In vitro	[23]
Encapsulated by photochromic compounds	NaYF4:Tm, Yb (28 nm)	$NaYF_4$, $mSiO_2$	Azobenzene	$NaYF_4$:Tm, Yb@$NaYF_4$@$mSiO_2$	DOX	HeLa cells	None	350, 450	In vitro	[22]

SiO_2: silica; M-540: merocyanine 540; MB: methylene blue; $mSiO_2$: mesoporous silica; ZnPc: zinc(II) phthalocyanine; TPPS2a: mesotetraphenylporphine with two sulfonate groups on adjacent phenyl rings; anti-STAT3: photomorpholino; Ce 6: Chlorin e6; DOX: doxorubicin; FA: folic acid; NB: nitrobenzyl; NBA: 2-nitrobenzylamine; DMNPE: 4,5-dimethoxy-2-nitroacetophenone; siRNA: small interfering RNA; PEG: polyethylene glycol; MCF-7/AZ cells: human breast cancer cells; MB49 cells: murine bladder cancer cells; B16-F0 cells: murine melanoma cells; HeLa cells: human epithelial carcinoma cells; A-498 cells: human kidney carcinoma cells; NIH/3 T3 cells: murine fibroblasts; A549 cells: human lung denocarcinoma epithelial cells; MRC-5 cells: normal human fibroblast cells; KB cells: human epithelial carcinoma cells.

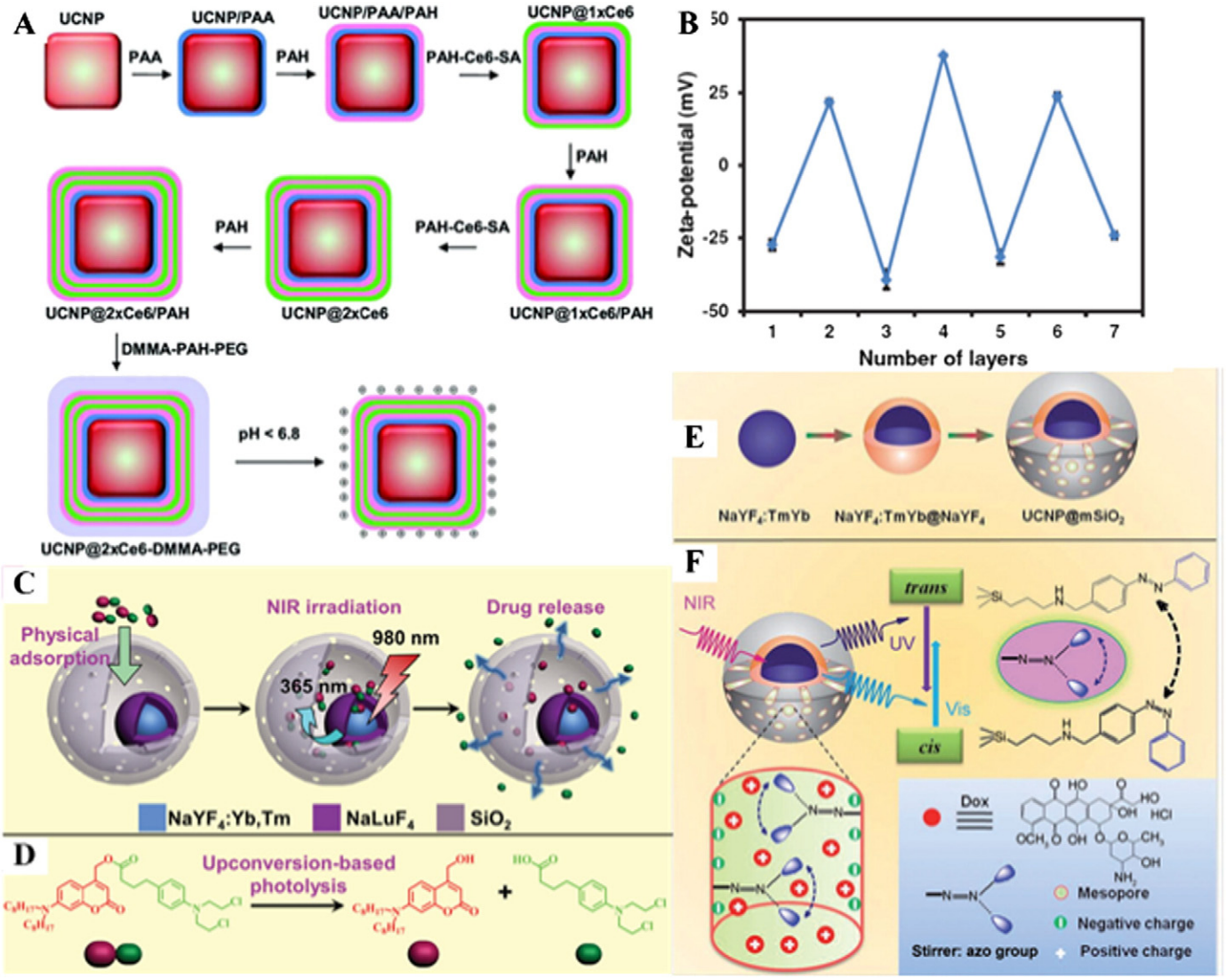

Fig. 3. Representative of advanced therapeutic payload encapsulation strategies. (A) Illustration of electrostatic attraction absorption based layer-by-layer assembly multi-layers of Ce6 encapsulation [26]. Reprinted with permission from Chao Wang, Liang Cheng, Yumeng Liu, Xiaojing Wang, Xinxing Ma, Zhaoyi Deng, Yonggang Li, Zhuang Liu, Advanced Functional Materials, 2013, 23(24), 3077–3086. Copyright 2013 John Wiley and Sons. (B) Zeta potentials of UCNPs via layer-by-layer assembly of increasing numbers of polymer coating layers and Ce6: 1) UCNP/PAA, 2) UCNP/PAA/PAH, 3) UCNP@1xCe6, 4) UCNP@1xCe6/PAH, 5) UCNP@2xCe6, 6) UCNP@2xCe6/PAH, and, 7) UCNP@3xCe6 [26].
Reprinted with permission from Chao Wang, Liang Cheng, Yumeng Liu, Xiaojing Wang, Xinxing Ma, Zhaoyi Deng, Yonggang Li, Zhuang Liu, Advanced Functional Materials, 2013, 23(24), 3077–3086. Copyright 2013 John Wiley and Sons. (C) Yolk–shell UCNPs loaded with photolabile group conjugated drug (amino-coumarin as photolabile group and chlorambucil as caged anticancer drug) [142]. (D) Cleavage of photolabile group conjugated drug [142]. Reprinted with permission from Lingzhi Zhao, Juanjuan Peng, Qi Huang, Chunyan Li, Min Chen, Yun Sun, Qiuning Lin, Linyong Zhu, Fuyou Li, Advanced Functional Materials, 2014, 24(3), 363–371. Copyright 2013 John Wiley and Sons. (E) Illustration of UCNP coated with a mesoporous silica layer [22]. (F) Anticancer drug doxorubicin was encapsulated by photochromic compound (azobenzene molecules) incorporated in the mesopore network of a mesoporous silica layer and phototriggered release [22]. Reprinted with permission from Jianan Liu, Wenbo Bu, Limin Pan, Jianlin Shi, Angewandte Chemie International Edition, 2013, 52(16), 4375–4379. Copyright 2013 John Wiley and Sons.

including chemotherapy, photodynamic therapy, and photothermal therapy.

3.1. UCNP-based NIR induced chemotherapy in cancer treatment

Chemotherapy is used to kill fast-growing cancer cells. To avoid its side effects and improve the therapeutic outcome, various delivery systems that are responsive to different stimuli (e.g., pH, redox environment, magnetic field, heat and light, electric field) have been developed to enable effective control over the delivery of cancer therapeutic payloads (drugs and biomolecules) [113,150–152]. Among all the above stimuli, light activated delivery systems allow temporal and spatial control over the delivery process. Traditional UV-based photoactivation systems, however, suffer from their intrinsic disadvantages associated with production of free radicals resulting in the development of skin cancer [153,154]. Limited penetration depth of UV also prevents such systems from in vivo applications. UCNPs as nanotransducers that can convert NIR excitation to UV emissions are very attractive in the engineering of NIR regulated delivery systems for cancer chemotherapy. Upon NIR excitation, the mild and localized upconverted UV emission generated by the UCNPs show minimal toxicity as compared with direct UV irradiation. Various UCN-based delivery systems capable of cancer chemotherapy have been developed using different technologies, such as photolysis of drug precursor or caged drug molecules and photoswitching of photochromic compound controlled release of drug molecules.

By photolysis of a drug precursor, Ford et al. prepared core–shell $NaYF_4$:Yb,Er@$NaYF_4$@SiO_2 UCNPs, which were then attached to Roussin's black salt anion $Fe_4S_3(NO)_7^-$ (RBS) by electrostatic interaction [155]. RBS was used as the precursor that generates tumor suppressing

NO (nitric oxide) under irradiation of NIR excitation due to the overlap between absorption of RBS and the upconversion emission at 550 nm of UCNPs. The same group further developed UCNPs and RBS systems in a biocompatible polymer disk device and demonstrated NO release under NIR excitation using porcine tissue as a filter [156]. These two studies, however, lacked in vitro demonstration. Shi et al. first carried out NIR induced in vitro chemotherapy on different cancer cell lines using photoswitching of photochromic compound controlled release of drug molecules [22]. They constructed a modified photochromic compound (azobenzene groups), mesoporous silica coated $NaYF_4$:TmYb UCNPs delivery system (Fig. 3 E, F). When the HeLa cells were treated by the prepared UCNPs loaded with or without anticancer drug (doxorubicin), negligible decrease in cell viability was observed, indicating inability to release doxorubicin to the cells in the absence of NIR excitation. Whereas, when irradiated at 980 nm, significantly increased cells death was observed resulting from unconverted UV (350 nm) and visible (450 nm) light induced reversible rotation–inversion movement of the azobenzene groups (trans–cis photoisomerization), triggering the release of anticancer molecules (Fig. 4 A, B). Similar cell killing effects were also found in L929 fibroblast cells, human embryonic kidney 293 T cells, U87 MG human glioblastoma cells, and murine 4 T1 breast cancer cells confirming the prospective of the UCNP-based NIR triggered photoswitching delivery system.

More recently, photolysis of caged drug molecules for NIR-controlled chemotherapy in living animal models has been reported [142]. In this study, the anticancer drug, chlorambucil was caged by the hydrophobized phototrigger of an aminocoumarin derivative (ACCh) and was then encapsulated into the yolk–shell $NaYF_4$:Yb,Tm@$NaLuF_4$ UCNPs (with silica as shell). The antitumor effect of the engineered yolk–shell delivery platform was tested both in vitro and in vivo in KB cells and in Kunming mice bearing injected S180 tumor masses (Fig. 4 C, D and E). A significant decrease in cell viability and tumor size were found in the groups treated with the UCNP-based photoactive yolk–shell delivery platform and irradiated with a NIR laser, while no change was observed in yolk–shell delivery platform treated only group (without NIR irradiation). This study demonstrated that remote NIR irradiation induced UV emission from UCNPs can effectively cleave the aminocoumarin derivative, resulting in the uncaging and releasing of the chlorambucil into tumor cells, and decrease the growth rate of tumors.

3.2. UCNP-based siRNA and DNA delivery in cancer treatment

Gene therapy by transfecting target cells with small interfering RNA (siRNA), plasmid DNA, or antisense oligonucleotides is one of the most promising strategies for gene-related diseases and cancer treatment [157]. Photoactivation has been applied for controlled gene expression and can be realized in two ways. The first way involves functionalization (or by physical absorption) of the nanoparticle using photocaged linkers bonded with siRNA. After internalization by target cells, upon UV irradiation, the photocaged linker could be cleaved initiating the intracellular release of the siRNA. Another approach to achieve improved photocontrol over intracellular gene release is photochemical internalization (PCI). PCI is a process that takes advantage of photoactivation of light-sensitive molecules encapsulated within the endosomes. The production of reactive oxygen species (ROS) by photoactivation of light-sensitive molecular disrupts the endosomal membrane and facilitates endosome escape, resulting in increase gene delivery efficiency [24,158]. The applications of UCNPs for NIR activated gene therapy are mostly based on these two methods and will be detailed below.

UCNP-based gene delivery system was first reported by Zhang and colleagues [159]. In their study, anti-Her2 antibody functionalized and GL3 luciferase siRNA loaded upconversion nanoparticles (UCNPs-Ab-siRNA) were used to transfect SK-BR-3 cells. The delivery system was demonstrated to successfully down-regulate luciferase gene expression by 45.5% while at the same time, their delivery could be tracked by fluorescence from UCNPs. This designed delivery system, however, was not able to track gene release from nanoplatform. To overcome this limitation, the same group applied fluorescence resonance energy transfer (FRET) analysis to study intracellular fate of siRNA, after their delivery into SK-BR-3 cells [160]. The FERT based delivery system was designed by using amine-modified silica coated UCNPs as the donor and siRNA–BOBO-3 complexes as the acceptor. The acceptor was physically adsorbed onto the donor. The detachment of siRNA–BOBO-3 complexes from the UCNPs resulted in decreased efficiency of the FRET process, indicating gradual release of siRNA into cells. Though this approach was able to real-time monitor the intracellular uptake, biostability of siRNA and remote control over intracellular release of siRNA in a highly spatial and temporal precision remains challenging.

Delivering siRNA in a controlled release manner by using photocaged linker method has been recently described [25]. A $NaYF_4$:Yb/Tm UCNP-based DNA/siRNA delivery system was developed for remote control and site-specific gene knockdown. In this study, the photoactive compound was applied to cage plasmid DNA and siRNA. The resulting complexes were loaded into the mesopores of silica layer surrounding UCNPs. Under NIR excitation, upconverted UV emission from UCNPs uncage plasmid DNA and siRNA from the compound to induce specific gene expression/down-regulation. Different thickness tissue phantom experiments on gene expression and knockdown of GFP demonstrated that the developed delivery platform holds great potential in gene therapy by controlled and site-specific gene delivery/knockdown (Fig. 5A–D). Without the need for chemical modification of delivered nucleic acids, Yang et al. designed simple and reliable NIR activatable nanoplatforms with higher payload of siRNA [23]. In their study, cationic photocaged linkers were covalently bonded to silica coated UNCPs. Anionic siRNA were absorbed onto cationic photocaged linkers through electrostatic attractions. Upon NIR irradiation, UNCPs converted the NIR to localized UV emission cleaving the photocaged linkers, facilitating the efficient release of siRNA for target gene silencing in vitro (Fig. 5E–L).

These platforms were successfully developed, but still suffer from poor endosomal escape, resulting in low gene knockdown capability. In another study, by photochemical internalization (PCI) method, Zhang et al. developed core–shell $NaYF_4$:Yb,Tm@$NaYF_4$:Yb,Er@nSiO_2@mSiO_2 UCNP-based nanoplatform for enhanced photocontrolled gene knockdown by improved endosomal escape (Fig. 6) [24]. The developed nanoplatform was simultaneously loaded with TPPS2a (a photosensitizer used in PCI) and a photomorpholino (anti-STAT3, short nucleic acid analogs for gene knockdown, becoming functional upon UV irradiation). After 980 nm NIR exposure, visible light at 413 nm (from $NaYF_4$:Yb,Er) photolysed TPPS2a to produce a ROS, locally disrupting the walls of the endosomal vesicles. Meanwhile, UV emission (from $NaYF_4$:Yb,Tm) resulted in the cleavage of the sense photomorpholino producing antisense photomorpholino and causing RNAi-mediated knockdown in the STAT3 gene. The system produced enhanced in vitro gene knockdown as much as 30% compared with the control without endosomal escape facilitation. The in vivo murine melanoma model demonstrated promising clinical potential of this system. Successful gene therapy relies on effective gene-delivery platforms. However, the complex spatial and temporal release of gene to take its function remains challenging. Therefore, controllable, efficient, and preferably traceable UCNP-based photoactivate gene delivery platforms have received intensive study in this area.

3.3. UCNP-based NIR induced photodynamic therapy in cancer treatment

Photodynamic therapy (PDT) has been a promising strategy for skin, lung, and neck and head cancer treatment [161–163]. Typical PDT is a two-step technique involving the use of photosensitizer (PS) molecules, followed activation with an appropriate wavelength of light. Upon light activation, PS molecules undergo photolysis, producing cytotoxic reactive oxygen species (ROS) and causing apoptosis or necrosis to surrounding cancer cells by destruction of biomolecules (e.g., proteins, lipids and

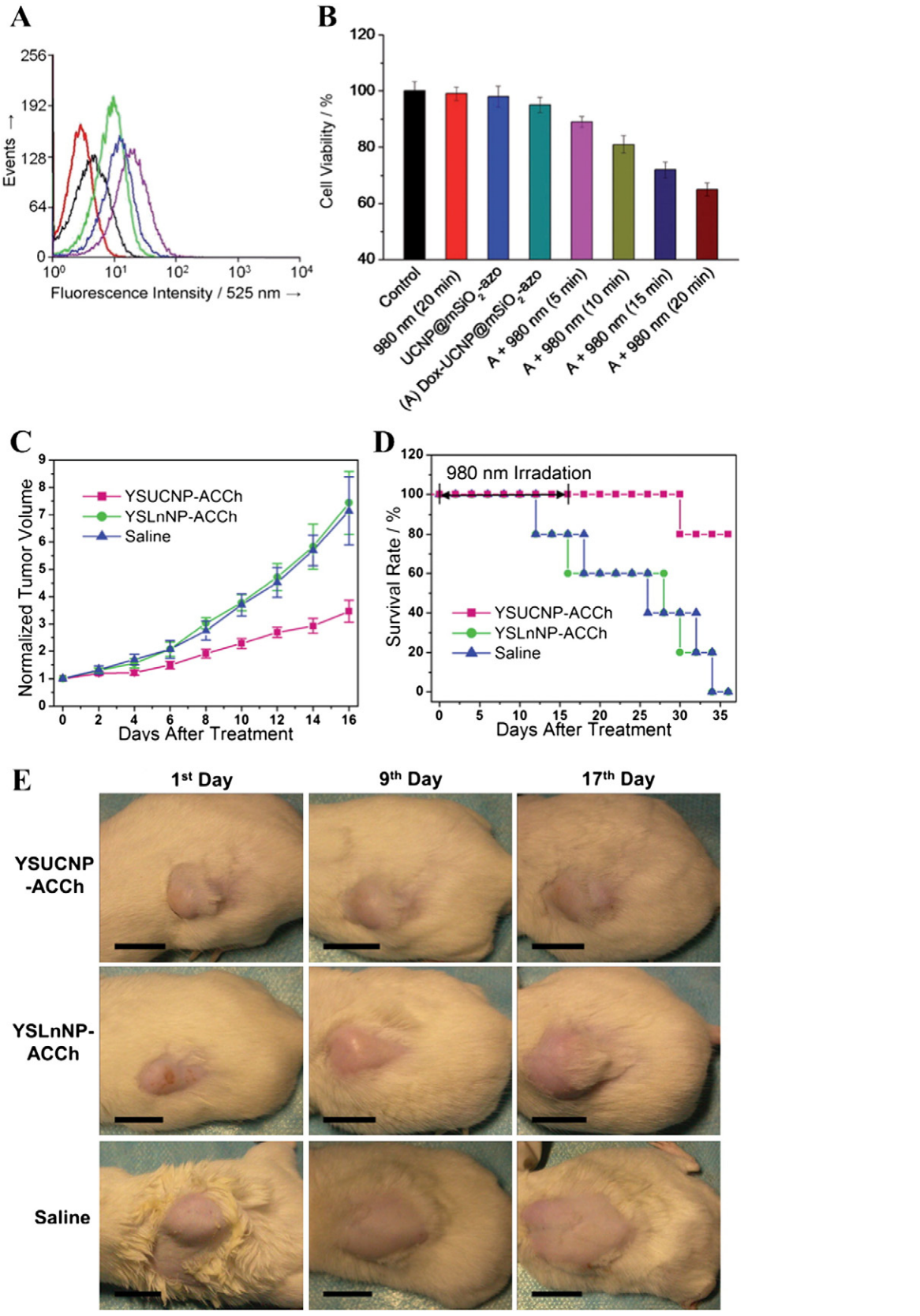

Fig. 4. Photoactivated chemotherapy in in vitro and in vivo studies. (A) Dox Fluorescence intensity of Dox in HeLa cell nuclei by flow cytometry histograms [22]. (B) HeLa cell growth inhibition with different treatments [22].
Reprinted with permission from Jianan Liu, Wenbo Bu, Limin Pan, Jianlin Shi, Angewandte Chemie International Edition, 2013, 52(16), 4375–4379. Copyright 2013 John Wiley and Sons. (C) Normalized tumor volume and (D) Mice survival rate with different treatments and subjected to different time periods. (E) Representative photos of mice with different treatments for different time periods. Scale bars: 1 cm [142]. Reprinted with permission from Lingzhi Zhao, Juanjuan Peng, Qi Huang, Chunyan Li, Min Chen, Yun Sun, Qiuning Lin, Linyong Zhu, Fuyou Li, Advanced Functional Materials, 2014, 24(3), 363–371. Copyright 2013 John Wiley and Sons.

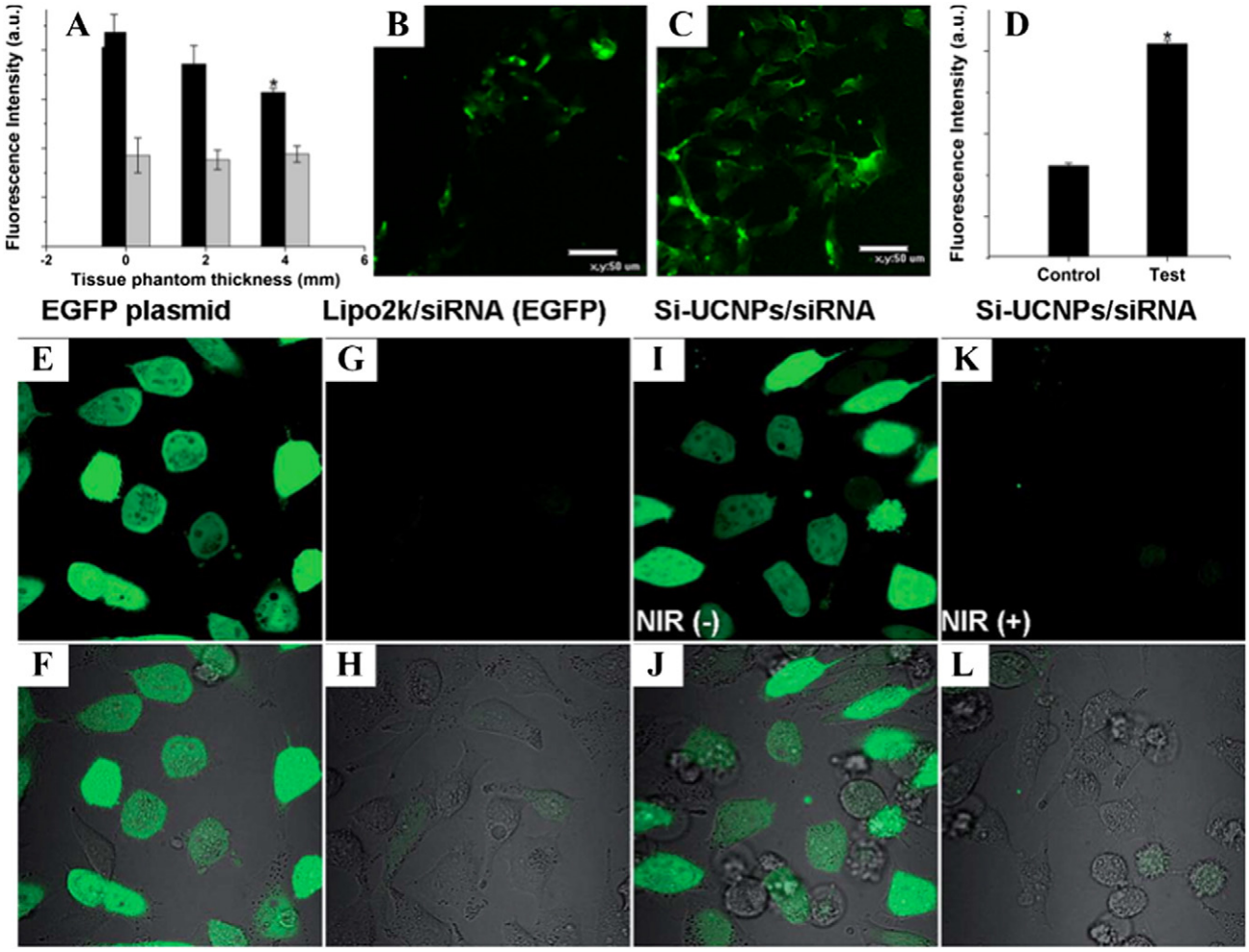

Fig. 5. Controlled gene release. Fluorescence intensity of GFP (transfected with UCNPs loaded with photocaged EGFP) in cells with (black) and without (gray) NIR irradiation through tissue phantoms of different thickness (A). In vitro result showing GFP expression in cells with (B) and without (C) NIR irradiation, respectively (scale bar, 50 μm). Quantified GFP fluorescence intensity (D) [25].
Reprinted with permission from Muthu Kumara Gnanasammandhan Jayakumar, Niagara Muhammad Idris, Yong Zhang, Proceedings of the National Academy of Sciences, 2012, 109(22), 8483–8488. Copyright 2012 Proceedings of the National Academy of Sciences. (E) Fluorescence and (F) overlapped bright field imaging of HeLa cells treated with EGFP plasmid. (G) Fluorescence and (H) overlapped bright field imaging for cells treated with Lipo2k/siRNA after EGFP plasmids transfection. UCNPs–siRNA complex treated cells, without NIR irradiation after EGFP plasmids transfection: (I) fluorescence image; (J) overlapped bright field image. UCNPs–siRNA complex treated cells, with NIR irradiation after EGFP plasmids transfection: (K) fluorescence image; (L) overlapped bright field image [23]. Reprinted with permission from Yanmei Yang, Fang Liu, Xiaogang Liu, Bengang Xing Nanoscale, 2013, 5(1), 231–238. Copyright 2012 Royal Society of Chemistry.

nucleic acids) [164–166]. There are several advantages associated with PDT including: (i) a non-invasive treatment method; and (ii) minimum damage to surrounding normal tissues by selected light activated treatment. Whereas, the disadvantages for conventional PDT lies in the requirement of UV light that results in poor tissue-penetration capacity and limiting the clinical application of PDT for large or internal tumors treatments.

UCNPs capable of converting NIR light into visible or UV photons have shown great promise in NIR light-induced PDT cancer treatment [121,124,134,167–169]. UCNP-based PDT employing NIR light as an activating source exhibited remarkably improved tissue penetration depth as compared with traditional PDT [170]. The pioneer work on the application of UCNP-based PDT in MCF-7/AZ bladder cancer cells was successfully developed by Zhang et al. [127]. In their study, they coated UCNPs with a thin layer of silica doped with PS, merocyanine-540. The obtained core–shell nanostructure was further functionalized with antibodies for targeted PDT upon NIR excitation. Though deeper tissue penetration was achieved, this delivery platform produced low efficiency in PDT due to the prohibited forming and releasing of ROS by non-porous silica layer. Through PEI-modified UCNPs bearing PS molecules, zinc phthalocyanine (ZnPc) facilitates forming and releasing of ROS, however, still resulted in low PS loading efficiency and leaking of PS from the UCNP surface [123,171]. To address these challenges, Zhang et al. [121,172,173] coated UCNPs with a mesoporous silica shell and loaded PS molecules into the porous shell. Both loading capacity and PDT efficiency were significantly improved. In a typical example of PDT for in vitro cancer cell treatment using the developed nanostructure, rapid ROS generation, followed by significant cell death were observed upon NIR irradiation with 980 nm light under power density of 500 mW for 5 min, indicating an improvement of PDT efficiency [172]. Similar works using mesoporous silica coated UCNPs as PS carrying vehicles also provided encouraging evidence for PDT applications [174,175].

In vivo photodynamic therapy using UCNPs as a remote controlled delivery platform has also been reported [121,134,169,176]. The ground work on in vivo UCNP-based NIR induced photodynamic therapy in cancer treatment was reported by Liu et al. [170] In their study, chlorin e6 (Ce6) was adsorbed on the surface of $NaYF_4$:Yb,Er UCNPs by hydrophobic interaction. The obtained complex was directly injected into the tumor sites and subjected to 980 nm NIR laser excitation. Although satisfactory tumor regression was observed, this design suffers from two

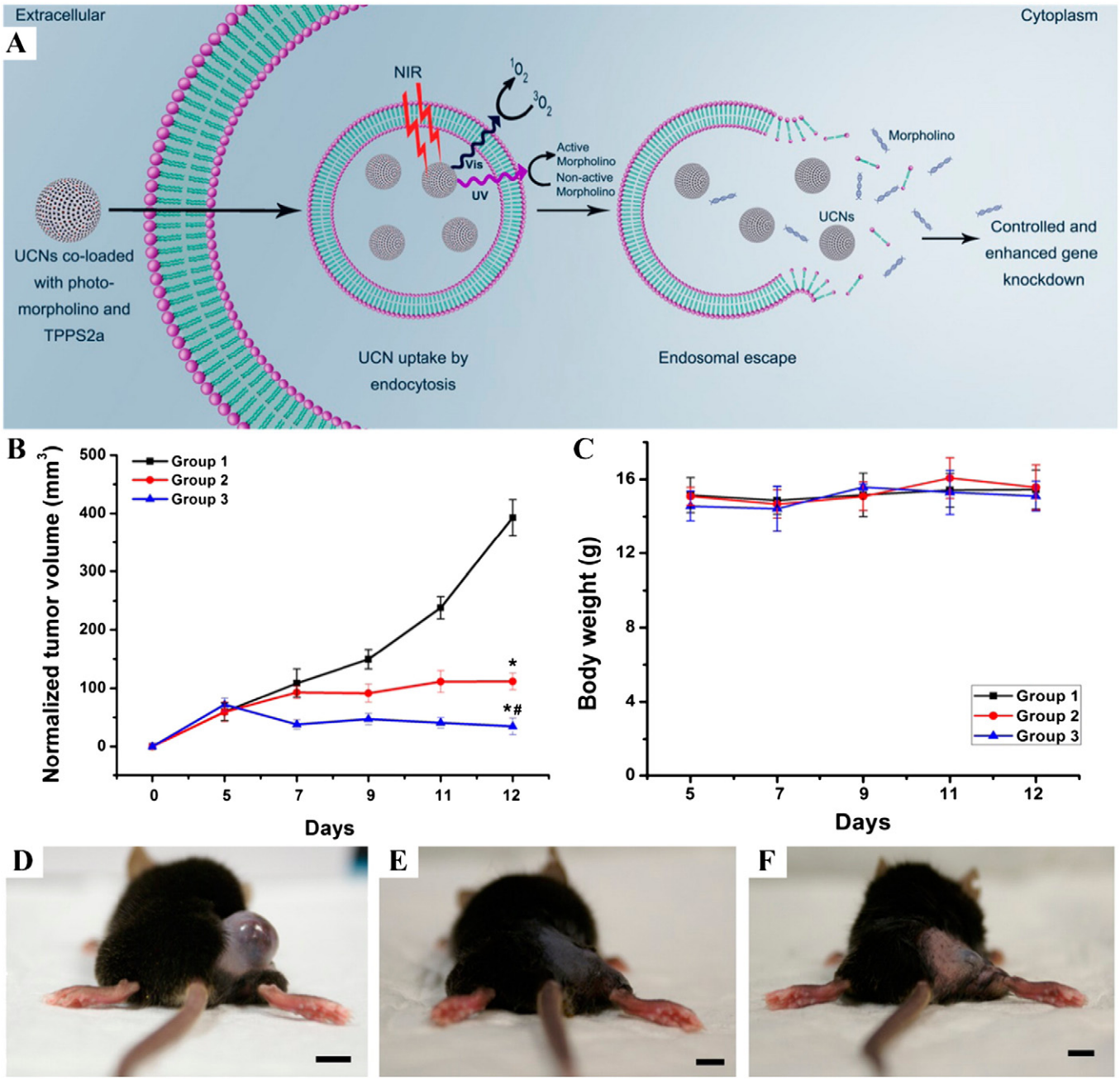

Fig. 6. Photochemical internalization with enhanced endosomal escape and gene knockdown. Schematic of UCNPs based photoactive delivery platform for endosomal escape and gene knockdown (A). Variation in tumor volume (B) and body weight (C) as a function of time as a consequence of STAT3 knockdown. (D) Saline control group. (E) UCNPs loaded with photomorpholinos under NIR irradiation. (F) UCNPs loaded both with photomorpholinos and TPPS2a under NIR irradiation. Scale bar: 1 cm [24].

disadvantages: (1) gradual dissociation of Ce6 molecules from UCNPs due to weak hydrophobic interactions; (2) weak red upconversion emission at around 660 nm from $NaYF_4$:Yb,Er was used to excite Ce6 molecules resulting in low PDT efficiency. In their later study, as opposed to $NaYF_4$:Yb,Er UCNPs, Mn^{2+} doped $NaYF_4$:Yb,Er,Mn UCNPs were employed to produce a strong single emission peak around 660 nm. In addition, two layers of Ce6 conjugated NaYF4:Yb/Er/Mn were achieved by a layer-by-layer assembly process (Fig. 3 A). The complex was further coated with pH-responsive charge reversible polymer. The surface of the final product can be converted to become positively charged in a tumor extracellular environment (pH 6.5–6.8), facilitating binding and internalization by tumor cells and significantly increasing PDT efficacy (Fig. 7 A). Those studies, however, lack of selective targeting capability to cancer cells. As opposed to loading with single PS, Zhang et al. proposed loading of two different kinds of PS, with one as ZnPc and the other as merocyanine 540 (MC540), each separately sensitive to 540 nm and 650 nm upconversion emission form $NaYF_4$:Yb,Er UCNPs [121]. In comparison to single PS loading, dual PS loading uses more efficient upconversion emission from UCNPs, generating improved ROS concentration and resulting in higher PDT efficacy. Moreover, the conjugation of dual PS loaded UCNPs with folic acid enables high accumulation of the complex into tumor areas through specific recognition of the receptors on the cancer cell allowing excellent tumor regression (Fig. 7 B, C).

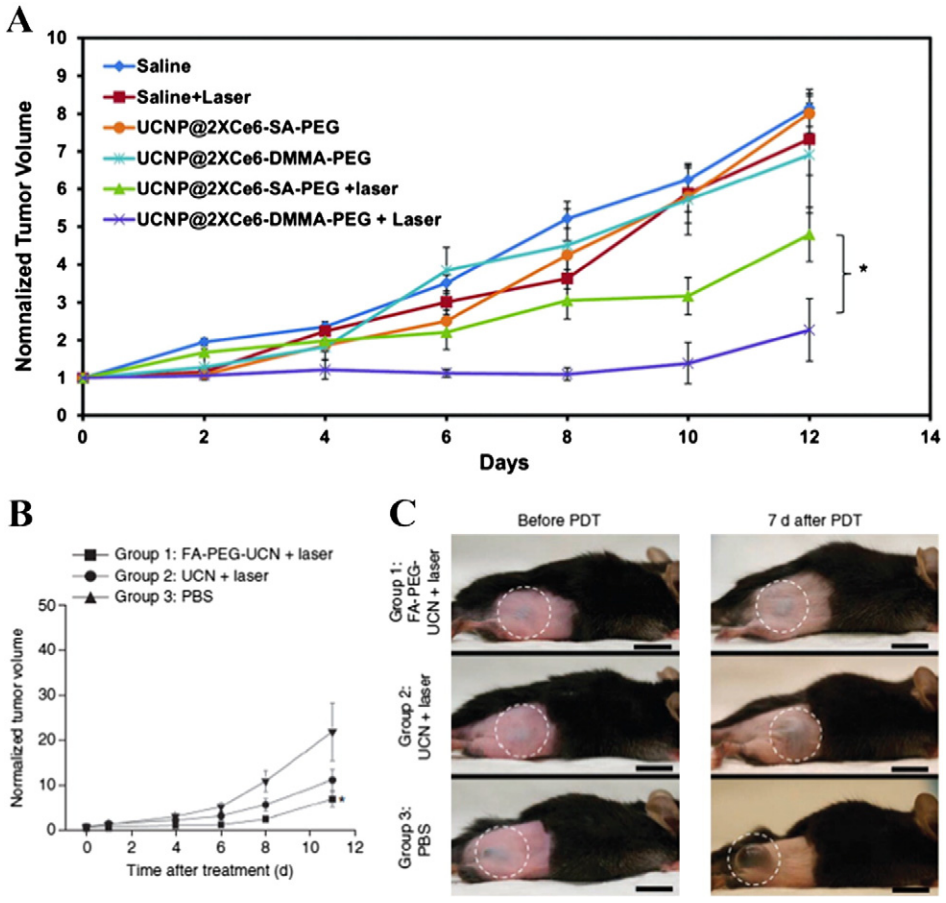

Fig. 7. In vivo PDT therapy. (A) Tumor growth after different treatments [26]. (B) Tumor volume change at different times after different treatments and (A) representative photos of mouse from different treatment groups showing the change in tumor volume before (0 d) and 7 d after PDT treatment. Scale bars, 10 mm [121].
Reprinted with permission from Niagara Muhammad Idris, Muthu Kumara Gnanasammandhan, Jing Zhang, Paul C Ho, Ratha Mahendran, Yong Zhang, Nature medicine, 2012, 18(10), 1580–1585. Copyright 2012 Nature Publishing Group.

3.4. UCNP-based NIR induced photothermal therapy in cancer treatment

Unlike PDT that utilizes a photosensitizer to generate cytotoxic ROS to kill cancer cells, photothermal therapy (PTT) is a treatment regime involving generation of heat from photoabsorbers leading to thermal ablation of cancer cells. Application of UCNPs in PTT that can be initiated by NIR irradiation has emerged as an increasingly recognized alternative to classical PTT involving using of UV as excitation source [177,178].

UCNPs have limited capability to convert light directly into heat due to low extinction coefficient of lanthanide ions. However, when coupled with other plasmonic nanoparticles (e.g., Ag, Au, and CuS) that have strong extinction coefficients, these UCNP-based nanocomposites shown great efficiency in PTT [29,179,180]. For example, silver-coated β-NaYF4:$Yb3^{+}/Er^{3+}$ core-shell structured nanoparticles have been designed for PTT. Their capability in PTT thermal ablation under NIR excitation was confirmed by in vitro experiments using both BCap-37 cells and HepG2 cells. The optimized PTT conditions with irradiation power density of 1.5 W/cm^2 led to tumor necrosis of up to 95% showing great potential as therapeutic agent for tumor ablation [179]. Via electrostatic attraction, ultrasmall superparamagnetic iron oxide (Fe_3O_4) nanoparticles were adsorbed on the surface of NaYF4:Yb^{3+}/Er^{3+} UCNPs to form a NaYF4:Yb^{3+}/Er^{3+}@ Fe_3O_4 complex [180]. The Au shell was subsequently formed on top of the complex by seed-induced reduction growth. After conjugating with folic acid through PEG linker, the engineered nanostructures were incubated with KB cells. After exposure to NIR laser at a power density of 1 W/cm^{-2} for 5 min, the majority of KB cells were killed. Very recently, in vivo application of UCNP-based PTT has been demonstrated by Shi et al. [29]. They developed a new type of multifunctional nanoplatform by decorating ultrasmall CuS nanoparticles as the satellites onto the surface of silica-coated UCNPs. By intratumoral injection, considerable tumor growth inhibition of 79% was observed after exposure to 980 nm NIR laser, confirming the potential of UCNPs@CuS as photothermal agents in vivo (Fig. 8A). Remarkably, UCNPs@CuS noncomplex was found to produce a synergistic effect of PTT thermal ablation and radiation therapy, confirmed by thoroughly eradicating tumors in four days without later recurrence for a prolonged period of up to 120 days (Fig. 8B).

Light controlled release upon UV irradiation holds great promise for optimizing therapeutic outcome through precise control of key factors, including specific site, timing, and desired dosage [181]. However, the major problem with this process is that UV irradiation is associated with phototoxic effects and low level of tissue penetration, thus prohibiting the designed delivery systems from in vivo applications. The advance in the engineering of UCNP-based delivery systems overcomes the limitations of using UV light as an excitation source, thus providing intriguing prospects for a new generation of photoactive delivery systems.

4. Concluding remarks and prospects

Photocoactive nanodelivery platforms provide great advances for spatially and temporally controlled release or activation of bioactive molecules (e.g., nucleic acids, drugs) by use of light of specific

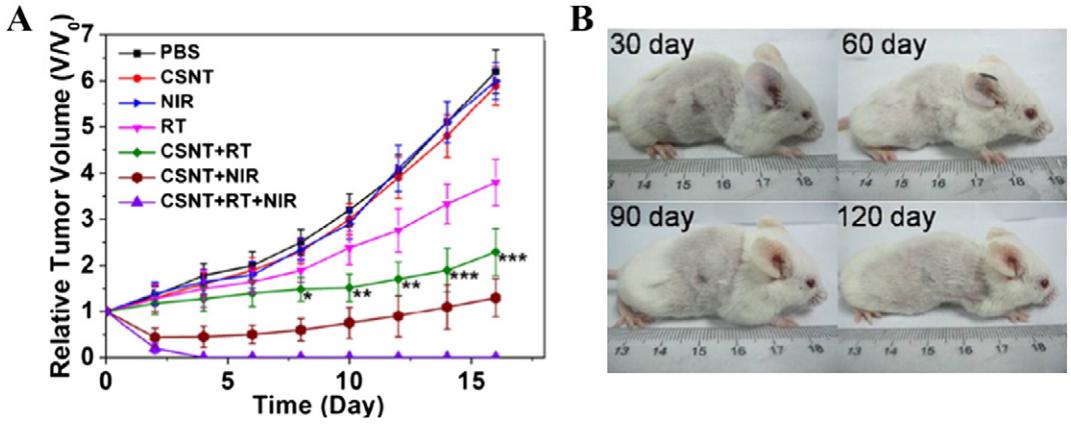

Fig. 8. In vivo synergistic therapeutic effects by injection with CSNTs in tumor site. Relative tumor volume as a function of time upon different treatments. (A). The representative photos of mouse after specific days of treatment showing the disappearance of the tumor and no further noticeable reappearance for 120 days (B) [29].
Reprinted with permission from Qingfeng Xiao, Xiangpeng Zheng, Wenbo Bu, Weiqiang Ge, Shengjian Zhang, Feng Chen, Huaiyong Xing, Qingguo Ren, Wenpei Fan, Kuaile Zhao, Yanqing Hua, and Jianlin Shi, Journal of the American Chemical Society, 2013, 135(35), 13,041–13,048. Copyright 2013 American Chemical Society.

wavelengths as external stimuli. The popular use of UV and visible light as external stimuli for traditional nanodelivery platform limit further clinical applications in consideration of damage of normal cells and limited tissue penetration depth. The emerging technologies for engineering of UCNP-based photocoactive nanodelivery platforms are able to convert deeper penetrating NIR light to localized UV or visible emission have shown great promise. In the past few years, numerous studies on UCNP-based photocoactive nanodelivery systems have been reported. Whereas, there are plenty of unresolved issues as identified below that need to be addressed for improved cancer theranotiscs.

4.1. Enhanced fluorescence intensity

Nanoparticles with sizes of less than 10 nm can be efficiently cleared from the body [182,183]. However, the smaller sized UCNPs are associated with low upconversion emission intensity limiting their clinical applications. In this regards, efforts are needed to design and synthesize UCNPs with enhanced upconversion emission intensity when their size is smaller than 10 nm [184]. For this end, various strategies have been developed to enhance fluorescence efficiency of UCNPs by materials design, including the optimization of doping ion concentration, host materials composition and phase, size, and morphology [65,82,98,183,185,186]. Plasmon effect on novel metals surface shows great potential to enhance fluorescence intensity of nearby fluorescent material [187]. Recently, our and other groups have demonstrated another promising plasmon-enhanced fluorescence strategy by modulating the distance between UCNPs and metal nanoparticles (i.e., Au and Ag) [188–190]. However, the exact underlying mechanism remains elusive and controlling their distance in nanoscale is still technically challenging. Further studies on plasmon-enhanced fluorescence technologies are required to explore the fluorescence enhancement mechanism and to fabricate high efficiency fluorescence system for photoactive applications.

4.2. Biocompatibility issue of UCNPs

Though functionalized UCNPs have been demonstrated to show good biocompatibility in in vitro cell experiments and in short term in vivo animal models [17,191–193], their long term toxicity effects, potential bioaccumulation, interaction with immune systems, and elimination pathways have not yet been investigated. Extensive and systematic evaluations are therefore required to eliminate biocompatibility concerns before those delivery platforms can finally be applied in clinic. Besides UCNPs, the biocompatibility of photoactive compounds applied for surface functionalization, such as azobenzene and o-nitrobenzyl derivatives are uncertain. Therefore, the synthesis or searching for substitute biocompatible photosensitive compounds will be critical in surface functionalization for advanced photoactivated cancer theranostics.

4.3. Multifunctionality of UCNPs

The engineering of UCNP core materials and elaborate surface functionalization are the key for disease diagnosis and treatments, as well as to achieve synergistic therapeutic effects. The performance of controlled delivery platform is strongly related to efficient NIR-to-UV by UCNPs. Therefore, it is of great importance to develop highly efficient NIR-to-UV UCNP cores. As for surface functionalization, most in vivo experiments are carried out by in situ tumor injection of nanomaterials due to the low accumulation concentration of nanomaterials at the specific tumor location when injected into mouse/rat tail intravenously. Therefore, the density of the targeting moieties on the surface of UCNPs needs to be optimized for improved real-time monitoring of treatment progress by tail intravenous injection. Furthermore, to achieve synergistic therapeutic effects, multi-payload encapsulation strategies via surface functionalization technologies need to be rigorously explored.

4.4. Tunability in emission and excitation

Continuous efforts are needed for designing upconversion emission and excitation with specific wavelengths [43]. For example, in deep-tissue imaging or tracking, NIR or red emission is preferred as they fall within the “biological window”, where both light absorption and scattering are negligible [194–196]. As opposed to NIR or red emission, strong UV–visible emissions are expected to perform photoactivated applications where UCNPs act as light converters by converting NIR excitation to localized UV–visible emissions [23,25,94,121,197]. Along with tuning in emission, the excitation wavelength also needs to be fine tuned. As discussed in this article, most of the UCNP-based photoactive delivery systems require an excitation wavelength of near 980 nm, which matches the absorption by the dopant sensitizer Yb^{3+} ions. This absorption peak, however, overlaps with the absorption peak of water, leading to an unexpected heat effect for long-term excitation or for high excitation power needed due to low upconversion emission efficiency. Therefore, it is of vital importance to develop UCNPs with excitation wavelengths in which water's heat absorption is negligible [95–97].

Acknowledgment

This study is supported in part, by grants from the Gategno and Wechsler funds (020572). Dr. Duan is supported, in part, through a grant from the Sarcoma Foundation of America (222433), a grant from the National Cancer Institute (NCI)/National Institutes of Health (NIH), UO1, CA 151452, and by the Fundamental Research Funds for the Central Universities (2012jdhz46). Dr. Lin is supported by a scholarship from the China Scholarship Council.

References

[1] Siegel R, Ma J, Zou Z, Jemal A. CA Cancer J Clin 2014;64:9–29.
[2] Zhu L, Perche F, Wang T, Torchilin VP. Biomaterials 2014;35:4213–22.
[3] Howell M, Mallela J, Wang C, Ravi S, Dixit S, Garapati U, et al. J Control Release 2013;167:210–8.
[4] Kesharwani P, Jain K, Jain NK. Prog Polym Sci 2014;39:268–307.
[5] Mignani S, El Kazzouli S, Bousmina M, Majoral JP. Adv Drug Deliv Rev 2013;65:1316–30.
[6] Du X, Shi B, Liang J, Bi J, Dai S, Qiao SZ. Adv Mater 2013;25:5981–5.
[7] Argyo C, Weiss V, Bräuchle C, Bein T. Chem Mater 2013;26:435–51.
[8] Kumar A, Zhang X, Liang X-J. Biotechnol Adv 2013;31:593–606.
[9] Ling D, Hyeon T. Small 2013;9:1450–66.
[10] Jiang S, Eltoukhy AA, Love KT, Langer R, Anderson DG. Nano Lett 2013;13:1059–64.
[11] Chen W, Zhong P, Meng F, Cheng R, Deng C, Feijen J, et al. J Control Release 2013;169:171–9.
[12] Huang Y-F, Chiang W-H, Huang W-C, Chen H-H, Shen M-Y, Lin S-C, et al. J Mater Chem B 2014;2:4988.
[13] Sun YL, Zhou Y, Li QL, Yang YW. Chem Commun (Camb) 2013;49:9033–5.
[14] Phillips DJ, Gibson MI. Antioxid Redox Signal 2013;21:786–803.
[15] Han G, You C-C, Kim B-j, Turingan RS, Forbes NS, Martin CT, et al. Angew Chem 2006;118:3237–41.
[16] Zhou J, Liu Z, Li FY. Chem Soc Rev 2012;41:1323–49.
[17] Chatterjee DK, Rufaihah AJ, Zhang Y. Biomaterials 2008;29:937–43.
[18] Idris NM, Li ZQ, Ye L, Sim EKW, Mahendran R, Ho PCL, et al. Biomaterials 2009;30:5104–13.
[19] Zhang F, Shi Q, Zhang Y, Shi Y, Ding K, Zhao D, et al. Adv Mater 2011;23:3775–9.
[20] Zhang C, Zhao K, Bu W, Ni D, Liu Y, Feng J, et al. Angew Chem 2014:n/an/a.
[21] Chien Y-H, Chou Y-L, Wang S-W, Hung S-T, Liau M-C, Chao Y-J, et al. ACS Nano 2013;7:8516–28.
[22] Liu J, Bu W, Pan L, Shi J. Angew Chem Int Ed 2013;52:4375–9.
[23] Yang Y, Liu F, Liu X, Xing B. Nanoscale 2013;5:231–8.
[24] Jayakumar MKG, Bansal A, Huang K, Yao R, Li BN, Zhang Y. ACS Nano 2014;8:4848–58.
[25] Jayakumar MKG, Idris NM, Zhang Y. Proc Natl Acad Sci 2012;109:8483–8.
[26] Wang C, Cheng L, Liu Y, Wang X, Ma X, Deng Z, et al. Adv Funct Mater 2013;23:3077–86.
[27] Wang X, Liu K, Yang G, Cheng L, He L, Liu Y, et al. Nanoscale 2014;6:9198–205.
[28] Chen F, Zhang S, Bu W, Chen Y, Xiao Q, Liu J, et al. Chem Eur J 2012;18:7082–90.
[29] Xiao Q, Zheng X, Bu W, Ge W, Zhang S, Chen F, et al. J Am Chem Soc 2013;135:13041–8.
[30] Gnach A, Lipinski T, Bednarkiewicz A, Rybkaab J, Capobiancod JA. Chem Soc Rev 2015;44:1561–84.
[31] Chen G, Qiu H, Prasad PN, Chen X. Chem Rev 2014;114:5161–214.
[32] Chen X, Peng DF, Ju Q, Wang F. Chem Soc Rev 2015;44:1318–30.
[33] Gu Z, Yan L, Tian G, Li S, Chai Z, Zhao Y. Adv Mater 2013;25:3758–79.
[34] Liu Q, Feng W, Li F. Coord Chem Rev 2014;273–274:100–10.
[35] Liu Q, Feng W, Yang T, Yi T, Li F. Nat Protoc 2013;8:2033–44.
[36] Shen J, Zhao L, Han G. Adv Drug Deliv Rev 2013;65:744–55.
[37] Sounderya N, Yong Z. Nanotechnology 2011;22:395101.
[38] Zheng W, Huang P, Tu DT, Ma E, Zhu HM, Chen XY. Chem Soc Rev 2015;44:1379–415.
[39] Li XM, Zhang F, Zhao DY. Chem Soc Rev 2015;44:1346–78.
[40] Idris NM, Jayakumar MK, Bansal A, Zhang Y. Chem Soc Rev 2015;44:1449–78.
[41] Yang D, Ma P, Hou Z, Cheng Z, Li C, Lin J. Chem Soc Rev 2015;44:1416–48.
[42] Cheng L, Wang C, Liu Z. Nanoscale 2013;5:23–37.
[43] Sun LD, Wang YF, Yan CH. Acc Chem Res 2014;47:1001–9.
[44] Murali Mohan Y, Vimala K, Thomas V, Varaprasad K, Sreedhar B, Bajpai SK, et al. J Colloid Interface Sci 2010;342:73–82.
[45] Wang F, Liu XG. Chem Soc Rev 2009;38:976–89.
[46] Lin M, Zhao Y, Wang S, Liu M, Duan Z, Chen Y, et al. Biotechnol Adv 2012;30:1551–61.
[47] Soukka T, Rantanen T, Kuningas K. Ann N Y Acad Sci 2008;1130:188–200.
[48] Yi GS, Chow GM. Chem Mater 2007;19:341–3.
[49] Boyer JC, Cuccia LA, Capobianco JA. Nano Lett 2007;7:847–52.
[50] Heer S, Kömpe K, Güdel HU, Haase M. Adv Mater 2004;16:2102–5.
[51] Chen G, Shen J, Ohulchanskyy TY, Patel NJ, Kutikov A, Li Z, et al. ACS Nano 2012;6:8280–7.
[52] Liu Q, Sun Y, Yang T, Feng W, Li C, Li F. J Am Chem Soc 2011;133:17122–5.
[53] Yin A, Zhang Y, Sun L, Yan C. Nanoscale 2010;2.
[54] Mai HX, Zhang YW, Sun LD, Yan CH. J Phys Chem C 2007;111:13721–9.
[55] Yi GS, Chow GM. Adv Funct Mater 2006;16:2324–9.
[56] Mai H-X, Zhang Y-W, Si R, Yan Z-G, Sun L-d, You L-P, et al. J Am Chem Soc 2006;128:6426–36.
[57] Boyer JC, Vetrone F, Cuccia LA, Capobianco JA. J Am Chem Soc 2006;128:7444–5.
[58] Zeng JH, Su J, Li ZH, Yan RX, Li YD. Adv Mater 2005;17:2119–23.
[59] Yan ZG, Yan CH. J Mater Chem 2008;18:5046–59.
[60] Wang LY, Zhang Y, Zhu YY. Nano Res 2010;3:317–25.
[61] Chuai XH, Zhang DS, Zhao D, Zheng K, He CF, Shi F, et al. Mater Lett 2011;65:2368–70.
[62] Du HY, Zhang WH, Sun JY. J Alloys Compd 2011;509:3413–8.
[63] Jin JF, Gu YJ, Man CWY, Cheng JP, Xu ZH, Zhang Y, et al. ACS Nano 2011;5:7838–47.
[64] Wang Y, Cai R, Liu Z. Cryst Eng Comm 2011;13:1772–4.
[65] Hao S, Chen G, Qiu H, Xu C, Fan R, Meng X, et al. Mater Chem Phys 2012;137:97–102.
[66] Su J, Zhang QL, Shao SF, Liu WP, Wan SM, Yin ST. J Alloys Compd 2009;470:306–10.
[67] Yi G, Lu H, Zhao S, Ge Y, Yang W, Chen D, et al. Nano Lett 2004;4:2191–6.
[68] Zheng W, Zhou S, Chen Z, Hu P, Liu Y, Tu D, et al. Angew Chem 2013;125:6803–8.
[69] Patra A, Friend CS, Kapoor R, Prasad PN. J Phys Chem B 2002;106:1909–12.
[70] Patra A, Friend CS, Kapoor R, Prasad PN. Chem Mater 2003;15:3650–5.
[71] Li CX, Quan ZW, Yang PP, Huang SS, Lian HZ, Lin J. J Phys Chem C 2008;112:13395–404.
[72] Quan ZW, Yang DM, Li CX, Kong DY, Yang PP, Cheng ZY, et al. Langmuir 2009;25:10259–62.
[73] Liu Y, Pisarski WA, Zeng S, Xu C, Yang Q. Opt Express 2009;17:9089–98.
[74] Qin X, Yokomori T, Ju YG. Appl Phys Lett 2007;90:073104.
[75] Gallini S, Jurado JR, Colomer MT. Chem Mater 2005;17:4154–61.
[76] Vu N, Kim Anh T, Yi GC, Strek W. J Lumin 2007;122-123:776–9.
[77] Liu Y, Tu D, Zhu H, Chen X. Chem Soc Rev 2013;42:6924–58.
[78] Feng SH, Xu RR. Acc Chem Res 2001;34:239–47.
[79] Huang P, Chen DQ, Wang YS. J Alloys Compd 2010;509:3375–81.
[80] Ma D-K, Huang S-M, Yu Y-Y, Xu Y-F, Dong Y-Q. J Phys Chem C 2009;113:8136–42.
[81] Tao Feng, Pan Feng, Wang Zhijun, Cai Weili, Yao L. Cryst Eng Comm 2010;12:4263–7.
[82] Zhuang J, Yang X, Fu J, Liang C, Wu M, Wang J, et al. Cryst Growth Des 2013;13:2292–7.
[83] Gao L, Ge X, Chai Z, Xu G, Wang X, Wang C. Nano Res 2009;2:565–74.
[84] Dou Q, Zhang Y. Langmuir 2011;27:13236–41.
[85] Qu X, Yang HK, Pan G, Chung JW, Moon BK, Choi BC, et al. Inorg Chem 2011;50:3387–93.
[86] Lin M, Zhao Y, Liu M, Qiu M, Dong Y, Duan Z, et al. J Mater Chem C 2014;2:3671–6.
[87] Zhang C, Sun L, Zhang Y, Yan C. J Rare Earths 2010;28:807–19.
[88] Wang M, Abbineni G, Clevenger A, Mao CB, Xu SK. Nanomed Nanotechnol Biol Med 2011;7:710–29.
[89] Wang F, Han Y, Lim CS, Lu Y, Wang J, Xu J, et al. Nature 2010;463:1061–5.
[90] Mahalingam V, Naccache R, Vetrone F, Capobianco JA. Chem Eur J 2009;15:9660–3.
[91] Feng AL, Lin M, Tian LM, Zhu HY, Guo H, Singamaneni S, et al. RSC Advances 2015;5:76825–35.
[92] Su Q, Han S, Xie X, Zhu H, Chen H, Chen C-K, et al. J Am Chem Soc 2012;134:20849–57.
[93] Du Y-P, Zhang Y-W, Sun L-D, Yan C-H. Dalton Trans 2009;3:8574–81.
[94] Qiu H, Chen G, Fan R, Yang L, Liu C, Hao S, et al. Nanoscale 2014;6:753–7.
[95] Xie X, Gao N, Deng R, Sun Q, Xu Q-H, Liu X. J Am Chem Soc 2013;135:12608–11.
[96] Wang Y-F, Liu G-Y, Sun L-D, Xiao J-W, Zhou J-C, Yan C-H. ACS Nano 2013;7:7200–6.
[97] Zhong Y, Tian G, Gu Z, Yang Y, Gu L, Zhao Y, et al. Adv Mater 2014;26:2831–7.
[98] Wang F, Deng R, Wang J, Wang Q, Han Y, Zhu H, et al. Nat Mater 2011;10:968–73.
[99] Wang F, Wang J, Liu X. Angew Chem 2010;122:7618–22.
[100] Shen J, Chen G, Ohulchanskyy TY, Kesseli SJ, Buchholz S, Li Z, et al. Small 2013;9:3213–7.
[101] Shen J, Chen G, Vu A-M, Fan W, Bilsel OS, Chang C-C, et al. Adv Opt Mater 2013;1:644–50.
[102] Zhou J, Shirahata N, Sun H-T, Ghosh B, Ogawara M, Teng Y, et al. J Phys Chem Lett 2013;4:402–8.
[103] Liu Y, Wang D, Shi J, Peng Q, Li Y. Angew Chem Int Ed 2013;52:4366–9.
[104] Cao T, Yang Y, Gao Y, Zhou J, Li Z, Li F. Biomaterials 2011;32:2959–68.
[105] Cao T, Yang Y, Sun Y, Wu Y, Gao Y, Feng W, et al. Biomaterials 2013;34:7127–34.
[106] Liu S, Han M-Y. Chem Asian J 2010;5:36–45.
[107] Piao Y, Burns A, Kim J, Wiesner U, Hyeon T. Adv Funct Mater 2008;18:3745–58.
[108] Johnson NJJ, Sangeetha NM, Boye JC, van Veggel FCJM. Nanoscale 2010;2:771–7.
[109] Li ZQ, Zhang Y. Angew Chem Int Ed 2006;45:7732–5.
[110] Fan W, Shen B, Bu W, Chen F, He Q, Zhao K, et al. Biomaterials 2014;35:8992–9002.
[111] Li C, Yang D, Pa Ma, Chen Y, Wu Y, Hou Z, et al. Small 2013;9:4150–9.
[112] Sun L, Wei Z, Chen H, Liu J, Guo J, Cao M, et al. Nanoscale 2014;6:8878–83.
[113] Graf N, Lippard SJ. Adv Drug Deliv Rev 2012;64:993–1004.
[114] Dai Y, Yang D, Ma Pa, Kang X, Zhang X, Li C, et al. Biomaterials 2012;33:8704–13.
[115] Chen Z, Chen H, Hu H, Yu M, Li F, Zhang Q, et al. J Am Chem Soc 2008;130:3023–9.
[116] Qiu HL, Chen GY, Sun L, Hao SW, Han G, Yang CH. J Mater Chem 2011;21:17202–8.
[117] Zhou J, Yu M, Sun Y, Zhang X, Zhu X, Wu Z, et al. Biomaterials 2011;32:1148–56.
[118] Zhou L, He B, Huang J, Cheng Z, Xu X, Wei C. ACS Appl Mater Interfaces 2014;6:7719–27.
[119] Esipova TV, Ye X, Collins JE, Sakadžić S, Mandeville ET, Murray CB, et al. Proc Natl Acad Sci 2012;109:20826–31.
[120] Cui S, Yin D, Chen Y, Di Y, Chen H, Ma Y, et al. ACS Nano 2012;7:676–88.
[121] Idris NM, Gnanasammandhan MK, Zhang J, Ho PC, Mahendran R, Zhang Y. Nat Med 2012;18:1580–5.
[122] Yang D, Kang X, Pa Ma, Dai Y, Hou Z, Cheng Z, et al. Biomaterials 2013;34 1601-12.
[123] Chatterjee DK, Zhang Y. Nanomedicine 2008;3:73–82.
[124] Liu K, Liu X, Zeng Q, Zhang Y, Tu L, Liu T, et al. ACS Nano 2012;6:4054–62.

[125] Wang X, Yang C-X, Chen J-T, Yan X-P. Anal Chem 2014;86:3263–7.
[126] Yuan Q, Wu Y, Wang J, Lu D, Zhao Z, Liu T, et al. Angew Chem 2013;125:14215–9.
[127] Zhang P, Steelant W, Kumar M, Scholfield M. J Am Chem Soc 2007;129:4526–7.
[128] Fan WP, Shen B, Bu WB, Zheng XP, He QJ, Cui ZW, et al. Biomaterials 2015;69:89–98.
[129] Liu JN, Bu WB, Shi JL. Acc Chem Res 2015;48:1797–805.
[130] Li X, Zhang J, Gu H. Langmuir 2011;28:2827–34.
[131] Guo H, Qian H, Idris NM, Zhang Y. Nanomedicine 2010;6:486–95.
[132] Yuan Q, Wu Y, Wang J, Lu D, Zhao Z, Liu T, et al. Angew Chem Int Ed Engl 2013;52:13965–9.
[133] Zeng L, Xiang L, Ren W, Zheng J, Li T, Chen B, et al. RSC Adv 2013;3:13915–25.
[134] Liu YY, Liu Y, Bu WB, Cheng C, Zuo ZJ, Xiao QF, et al. Angew Chem Int Ed 2015;127:8223–7.
[135] Wang C, Cheng L, Liu Z. Theranostics, 3; 2013 317–30.
[136] Yang Y, Velmurugan B, Liu X, Xing B. Small 2013;9:2937–44.
[137] Yang Y, Shao Q, Deng R, Wang C, Teng X, Cheng K, et al. Angew Chem Int Ed 2012;51:3125–9.
[138] Carling CJ, Nourmohammadian F, Boyer JC, Branda NR. Angew Chem Int Ed 2010;49:3782–5.
[139] Yan B, Boyer J-C, Habault D, Branda NR, Zhao Y. J Am Chem Soc 2012;134:16558–61.
[140] Yan B, Boyer J-C, Branda NR, Zhao Y. J Am Chem Soc 2011;133:19714–7.
[141] Li W, Wang J, Ren J, Qu X. J Am Chem Soc 2014;136:2248–51.
[142] Zhao L, Peng J, Huang Q, Li C, Chen M, Sun Y, et al. Adv Funct Mater 2014;24:363–71.
[143] Mura S, Nicolas J, Couvreur P. Nat Mater 2013;12:991–1003.
[144] Zhou L, Chen Z, Dong K, Yin M, Ren J, Qu X. Adv Mater 2014;26:2424–30.
[145] Carling CJ, Boyer JC, Branda NR. J Am Chem Soc 2009;131:10838–9.
[146] Boyer JC, Carling CJ, Gates BD, Branda NR. J Am Chem Soc 2010;132:15766–72.
[147] Yang T, Liu Q, Li J, Pu S, Yang P, Li F. RSC Adv 2014;4:15613–9.
[148] Zhang BF, Frigoli M, Angiuli F, Vetrone F, Capobianco JA. Chem Commun (Camb) 2012;48:7244–6.
[149] Wang L, Dong H, Li Y, Xue C, Sun LD, Yan CH, et al. J Am Chem Soc 2014;136:4480–3.
[150] Liu J, Huang Y, Kumar A, Tan A, Jin S, Mozhi A, et al. Biotechnol Adv 2014;32:693–710.
[151] Hijnen N, Langereis S, Grüll H. Adv Drug Deliv Rev 2014;72:65–81.
[152] Akimoto J, Nakayama M, Okano T. J Control Release 2014;193:2–8.
[153] Cheng L, Wang C, Feng L, Yang K, Liu Z. Chem Rev 2014;114:10869–939.
[154] Bansal A, Zhang Y. Acc Chem Res 2014;47:3052–60.
[155] Garcia JV, Yang J, Shen D, Yao C, Li X, Wang R, et al. Small 2012;8:3800–5.
[156] Burks PT, Garcia JV, GonzalezIrias R, Tillman JT, Niu M, Mikhailovsky AA, et al. J Am Chem Soc 2013;135:18145–52.
[157] Tan SJ, Kiatwuthinon P, Roh YH, Kahn JS, Luo D. Small 2011;7:841–56.
[158] Mellert K, Lamla M, Scheffzek K, Wittig R, Kaufmann D. PLoS One 2012;7, e52473.
[159] Shan J, Yong Z, Kian Meng L, Eugene KWS, Lei Y. Nanotechnology 2009;20:155101.
[160] Jiang S, Zhang Y. Langmuir 2010;26:6689–94.
[161] Master A, Livingston M, Sen Gupta A. J Control Release 2013;168:88–102.
[162] Master AM, Livingston M, Oleinick NL, Sen Gupta A. Mol Pharm 2012;9:2331–8.
[163] Master AM, Qi Y, Oleinick NL, Gupta AS. Nanomed: Nanotechnol, Biol Med 2012;8655-64.
[164] Robertson CA, Evans DH, Abrahamse H. J Photochem Photobiol B Biol 2009;96:1–8.
[165] Castano AP, Mroz P, Hamblin MR. Nat Rev Cancer 2006;6:535–45.
[166] Oleinick NL, Morris RL, Belichenko I. Photochem Photobiol Sci 2002;1:1–21.
[167] Wang H, Dong C, Zhao P, Wang S, Liu Z, Chang J. Int J Pharm 2014;466:307–13.
[168] Chatterjee DK, Gnanasammandhan MK, Zhang Y. Small 2010;6:2781–95.
[169] Park YI, Kim HM, Kim JH, Moon KC, Yoo B, Lee KT, et al. Adv Mater 2012;24:5755–61.
[170] Wang C, Tao H, Cheng L, Liu Z. Biomaterials 2011;32:6145–54.
[171] Lim ME, Lee Y-l, Zhang Y, Chu JJH. Biomaterials 2012;33:1912–20.
[172] Qian HS, Guo HC, Ho PC-L, Mahendran R, Zhang Y. Small 2009;5:2285–90.
[173] Guo H, Qian H, Idris NM, Zhang Y. Nanomed: Nanotechnol, Biol Med 2010;6:486–95.
[174] Qiao X-F, Zhou J-C, Xiao J-W, Wang Y-F, Sun L-D, Yan C-H. Nanoscale 2012;4:4611–23.
[175] Liu X, Qian H, Ji Y, Li Z, Shao Y, Hu Y, et al. RSC Adv 2012;2:12263–8.
[176] Xia L, Kong X, Liu X, Tu L, Zhang Y, Chang Y, et al. Biomaterials 2014;35:4146–56.
[177] Cheng L, Yang K, Li Y, Zeng X, Shao M, Lee S-T, et al. Biomaterials 2012;33:2215–22.
[178] Qian L, Zhou L, Too H-P, Chow G-M. J Nanoparticle Res 2011;13:499–510.
[179] Dong B, Xu S, Sun J, Bi S, Li D, Bai X, et al. J Mater Chem 2011;21:6193.
[180] Cheng L, Yang K, Li Y, Chen J, Wang C, Shao M, et al. Angew Chem 2011;123:7523–8.
[181] Alvarez-Lorenzo C, Bromberg L, Concheiro A. Photochem Photobiol 2009;85:848–60.
[182] Wong H-T, Vetrone F, Naccache R, Chan HLW, Hao J, Capobianco JA. J Mater Chem 2011;21:16589–96.
[183] Chen G, Ohulchanskyy TY, Kumar R, Ågren H, Prasad PN. ACS Nano 2010;4:3163–8.
[184] Han S, Deng R, Xie X, Liu X. Angew Chem Int Ed 2014:n/an/a.
[185] Chen D, Yu Y, Huang F, Wang Y. Chem Commun 2011;47:2601–3.
[186] Wang F, Wang J, Liu X. Angew Chem Int Ed 2010;49:7456–60.
[187] Gandra N, Portz C, Tian L, Tang R, Xu B, Achilefu S, et al. Angew Chem 2013;125:1–6.
[188] Greybush NJ, Saboktakin M, Ye X, Della Giovampaola C, Oh SJ, Berry NE, et al. ACS Nano 2014;8 (9482-91).
[189] Feng AL, You ML, Tian LM, Singamaneni S, Liu M, Duan ZF, et al. Sci Rep 2015;5:7779.
[190] Saboktakin M, Ye X, Oh SJ, Hong S-H, Fafarman AT, Chettiar UK, et al. ACS Nano 2012;6:8758–66.
[191] Xiong L, Yang T, Yang Y, Xu C, Li F. Biomaterials 2010;31:7078–85.
[192] Cheng L, Yang K, Shao M, Lu X, Liu Z. Nanomedicine 2011;6:1327–40.
[193] Abdul Jalil R, Zhang Y. Biomaterials 2008;29:4122–8.
[194] Wang J, Wang F, Wang C, Liu Z, Liu X. Angew Chem Int Ed 2011;50:10369–72.
[195] Chan EM, Han G, Goldberg JD, Gargas DJ, Ostrowski AD, Schuck PJ, et al. Nano Lett 2012;12:3839–45.
[196] Li Z-X, Li L-L, Zhou H-P, Yuan Q, Chen C, Sun L-D, et al. Chem Commun (Camb) 2009:6616–8.
[197] Wang L, Lan M, Liu Z, Qin G, Wu C, Wang X, et al. J Mater Chem C 2013;1:2485–90.